JOURNAL OF GEOPHYSICAL RESEARCH, VOL. 114, D10306, doi:10.1029/2008JD010984, 2009

Effect of chemistry-aerosol-climate coupling on predictions of future climate and future levels of tropospheric ozone and aerosols

Hong Liao,[1] Ying Zhang,[1] Wei-Ting Chen,[2] Frank Raes,[3] and John H. Seinfeld[2,4]

Received 14 August 2008; revised 20 February 2009; accepted 3 March 2009; published 23 May 2009.

[1] We explore the extent to which chemistry-aerosol-climate coupling influences predictions of future ozone and aerosols as well as future climate using the Goddard Institute for Space Studies (GISS) general circulation model II' with on-line simulation of tropospheric ozone-NO_x-hydrocarbon chemistry and sulfate, nitrate, ammonium, black carbon, primary organic carbon, and secondary organic carbon aerosols. Based on IPCC scenario A2, year 2100 ozone, aerosols, and climate simulated with full chemistry-aerosol-climate coupling are compared with those simulated from a stepwise approach. In the stepwise method year 2100 ozone and aerosols are first simulated using present-day climate and year 2100 emissions (denoted as simulation CHEM2100sw) and year 2100 climate is then predicted using offline monthly fields of O_3 and aerosols from CHEM2100sw (denoted as simulation CLIM2100sw). The fully coupled chemistry-aerosol-climate simulation predicts a 15% lower global burden of O_3 for year 2100 than the simulation CHEM2100sw which does not account for future changes in climate. Relative to CHEM2100sw, year 2100 column burdens of all aerosols in the fully coupled simulation exhibit reductions of 10–20 mg m^{-2} in DJF and up to 10 mg m^{-2} in JJA in mid to high latitudes in the Northern Hemisphere, reductions of up to 20 mg m^{-2} over the eastern United States, northeastern China, and Europe in DJF, and increases of 30–50 mg m^{-2} over populated and biomass burning areas in JJA. As a result, relative to year 2100 climate simulated from CLIM2100sw, full chemistry-aerosol-climate coupling leads to a stronger net global warming by greenhouse gases, tropospheric ozone and aerosols in year 2100, with a global and annual mean surface air temperature higher by 0.42 K. For simulation of year 2100 aerosols, we conclude that it is important to consider the positive feedback between future aerosol direct radiative forcing and future aerosol concentrations; increased aerosol concentrations lead to reductions in convection and precipitation (or wet deposition of aerosols), further increasing lower tropospheric aerosol concentrations.

Citation: Liao, H., Y. Zhang, W.-T. Chen, F. Raes, and J. H. Seinfeld (2009), Effect of chemistry-aerosol-climate coupling on predictions of future climate and future levels of tropospheric ozone and aerosols, *J. Geophys. Res.*, *114*, D10306, doi:10.1029/2008JD010984.

1. Introduction

[2] Chemistry-aerosol-climate interactions influence abundances of tropospheric O_3 and aerosols (hereafter referred to as O_3&AERs) and their radiative forcing of climate. Gas-phase species determine the formation and growth of aerosols, and aerosols influence gas-phase chemistry by serving as sites for heterogeneous reactions [*Dentener and Crutzen*, 1993; *Jacob*, 2000; *Liao and Seinfeld*, 2005] and by altering gas-phase photolysis rates [*Jacobson*, 1998; *Liao et al.*, 1999]. Although growth in levels of well-mixed, long-lived greenhouse gases (GHGs, including CO_2, CH_4, N_2O, and halocarbons) in the atmosphere is the dominant contributor to climate change, tropospheric O_3&AERs have made significant contributions to radiative forcing of climate since preindustrial times [*Intergovernmental Panel on Climate Change* (*IPCC*), 2007]. Ozone is a greenhouse gas; aerosols influence climate through absorption and scattering of radiation (the so-called direct effect) and through their influence on cloud properties (the so-called indirect effect). Furthermore, climate change affects concentrations of tropospheric O_3&AERs by influencing natural emissions, chemical reactions, transport, and deposition. These interactions complicate estimation of concentrations of O_3&AERs as well as climate change on decadal and longer time scales.

[1] State Key Laboratory of Atmospheric Boundary Layer Physics and Atmospheric Chemistry, Institute of Atmospheric Physics, Chinese Academy of Sciences, Beijing, China.
[2] Department of Environmental Science and Engineering, California Institute of Technology, Pasadena, California, USA.
[3] European Commission, Joint Research Center, Ispra, Italy.
[4] Department of Chemical Engineering, California Institute of Technology, Pasadena, California, USA.

0148-0227/09/2008JD010984$09.00

[3] Simulations of future O_3&AERs in previous studies usually take one of the following two approaches. One approach is to estimate future levels based on present-day climate and projected emissions of ozone precursors and aerosols/aerosol precursors [e.g., *Adams et al.*, 2001; *Koch*, 2001; *Iversen and Seland*, 2002; *Liao and Seinfeld*, 2005; *Horowitz*, 2006], in which the impact of climate change on O_3&AERs is not considered. Another approach is to simulate future O_3&AERs accounting for projected GHG increases and future changes in non-GHG anthropogenic emissions. A warmer climate is predicted to alter natural emissions of ozone precursors, such as biogenic hydrocarbons [*Sanderson et al.*, 2003; *Lathière et al.*, 2005; *Guenther et al.*, 2006; *Wiedinmyer et al.*, 2006; *Liao et al.*, 2006] and NO_x from lightning and soil [*Price and Rind*, 1992; *Liao et al.*, 2006; *Wu et al.*, 2008], to reduce the tropospheric burden of ozone as a result of increased temperature and water vapor [*Johnson et al.*, 2001; *Brasseur et al.*, 1998, 2006; *Unger et al.*, 2006; *Liao et al.*, 2006; *Murazaki and Hess*, 2006], and to increase O_3 concentrations over or near populated and biomass burning areas because of slower transport, enhanced biogenic hydrocarbon emissions, and decomposition of peroxyacetyl nitrate at higher temperatures [*Hogrefe et al.*, 2004; *Liao et al.*, 2006; *Steiner et al.*, 2006; *Murazaki and Hess*, 2006; *Wu et al.*, 2008; *Racherla and Adams*, 2008]. While changes in meteorological fields have impacts on emissions of natural aerosols/aerosol precursors (e.g. dimethylsulfide (DMS), biogenic hydrocarbons, sea salt, and mineral dust), a warmer climate influences aerosol levels through altered concentrations of atmospheric oxidants, precipitation, boundary layer height, and by shifting gas-particle equilibria [*Unger et al.*, 2006; *Liao et al.*, 2006; *Bauer et al.*, 2007; *Pye et al.*, 2009]. The studies cited above underscore the important role of climate change in predictions of future O_3&AERs. In previous studies, however, the complete feedback effect has not been considered, namely the radiative effect of simulated O_3&AERs was not fed back into the climate simulation and consequently fed back into simulation of O_3&AERs themselves. We present the results of such a study here.

[4] There are numerous assessments of climate change driven by tropospheric ozone [e.g., *Ramaswamy and Bowen*, 1994; *Hansen et al.*, 1997; *Stuber et al.*, 2001; *Mickley et al.*, 2004; *Shindell et al.*, 2006a, 2006b; *Chen et al.*, 2007] and aerosols [*Hansen et al.*, 1997; *Boer et al.*, 2000; *Chung et al.*, 2002; *Menon et al.*, 2002; *Jacobson*, 2004; *Wang*, 2004, 2007; *Chung and Seinfeld*, 2005; *Hansen et al.*, 2005; *Ramanathan et al.*, 2005; *Takemura et al.*, 2005; *Stier et al.*, 2006; *Roeckner et al.*, 2006; *Chen et al.*, 2007; *Shindell et al.*, 2008]. A stepwise method has commonly been used in previous studies to simulate climate change driven by O_3&AERs [e.g., *Boer et al.*, 2000; *Mickley et al.*, 2004; *Hansen et al.*, 2005; *Chen et al.*, 2007; *Levy et al.*, 2008]. In the stepwise approach generally the first step is to simulate preindustrial or future concentrations of O_3&AERs based on present-day climate and changes in non-GHG anthropogenic emissions. The second step is to use these concentrations of O_3&AERs simulated *a priori* in the radiative transfer module of a general circulation model (GCM) to drive climate change, with levels of O_3&AERs fixed during the climate simulation. Such stepwise simulations do not account for the changes in concentrations of O_3&AERs as the climate itself is perturbed.

[5] We explore here the extent to which chemistry-aerosol-climate coupling influences predictions of future O_3&AERs as well as future climate itself. We utilize a unified tropospheric chemistry-aerosol model within the Goddard Institute for Space Studies general circulation model II' (GISS GCM II') [*Liao et al.*, 2003, 2004]. The model includes a detailed simulation of tropospheric O_3-NO_x-hydrocarbon chemistry, as well as aerosol precursors and aerosols (sulfate, nitrate, ammonium, black carbon (BC), primary organic carbon (POA), secondary organic carbon (SOA), sea salt, and mineral dust). We have applied the model to understand the radiative effect of O_3&AERs on future climate in the stepwise manner described above [*Chen et al.*, 2007]. The goal of this work is to quantify: (1) differences between year 2100 climate predicted in a fully-coupled simulation and that using the stepwise approach and (2) for simulation of future O_3&AERs, besides consideration of future climate change driven by GHGs, assess the importance of future climate change driven by O_3&AERs themselves. It should be noted that we consider only the direct radiative effect of aerosols in this work; the indirect radiative effect of aerosols will be the subject of future work.

2. Model Description and Experiments

2.1. Unified Model

[6] The unified tropospheric chemistry-aerosol model within the GISS GCM II' is described in detail in previous studies [*Liao et al.*, 2003, 2004; *Liao and Seinfeld*, 2005; *Liao et al.*, 2006]. The GISS GCM II' has a horizontal resolution of 4° latitude by 5° longitude, with 9 σ vertical layers from surface to 10 mb [*Rind and Lerner*, 1996; *Rind et al.*, 1999] and is coupled with a "Q-flux" ocean [*Hansen et al.*, 1984]. In the Q-flux ocean, monthly horizontal heat transport fluxes are held constant as in *Mickley et al.* [2004], while changes in the sea surface temperature and sea ice are calculated based on energy exchange with the atmosphere, ocean heat transport, and the ocean mixed layer heat capacity [*Hansen et al.*, 1984; *Russell et al.*, 1984]. The GISS model has been used extensively to probe the climate response to perturbations in GHG concentrations, solar luminosity, and tropospheric O_3 and aerosol burdens [e.g. *Grenfell et al.*, 2001; *Rind et al.*, 2001; *Shindell et al.*, 2001; *Menon*, 2004; *Mickley et al.*, 2004; *Chung and Seinfeld*, 2005; *Chen et al.*, 2007].

[7] The model includes a detailed simulation of tropospheric O_3-NO_x-hydrocarbon chemistry, as well as sulfate, nitrate, ammonium, BC, POA, SOA, sea salt, and mineral dust aerosols. Upper boundary layer conditions for O_3 and NO_x are applied at the tropopause (about 150 hPa) to represent transport across the tropopause, as described by *Wang et al.* [1998]. The chemical mechanism includes 225 chemical species and 346 reactions for simulating gas-phase species and aerosols. The partitioning of ammonia and nitrate between gas and aerosol phases is determined by the on-line thermodynamic equilibrium model ISORROPIA [*Nenes et al.*, 1998], and the formation of secondary organic aerosol from monoterpenes is based on equilibrium partitioning and experimentally determined yield parameters [*Griffin et al.*, 1999a, 1999b; *Chung and Seinfeld*, 2002].

Table 1. Global and Annual Anthropogenic Emissions of O_3 Precursors, Aerosols/Aerosol Precursors for Present-Day and 2100[a]

Species	Scenario	
	Present-day	2100 (IPCC SRES A2)
NO_x (Tg N yr^{-1})	32	109.7
CO (Tg CO yr^{-1})	1030	2498
Ethane (Tg C yr^{-1})	8.6	100.1
Propane (Tg C yr^{-1})	6.7	28.1
$\geq C_4$ alkanes (Tg C yr^{-1})	30.1	60.5
$\geq C_3$ alkenes (Tg C yr^{-1})	22	41
Acetone (Tg C yr^{-1})	9	9
SO_2 (Tg S yr^{-1})	71.3	62.6
NH_3 (Tg N yr^{-1})	46.9	102.6
POA (Tg OM yr^{-1})	82.2	189.5
BC (Tg C yr^{-1})	12.2	28.8

[a]See *Liao et al.* [2006] for sources of emissions of different species.

(The simulation of secondary organic aerosol does not include isoprene or more recent laboratory yields; these will be updated in future work. For the present study, the effect of the ''missing'' organic aerosol should not be significant.) Two-way coupling between aerosols and gas-phase chemistry provides consistent chemical fields for aerosol dynamics and aerosol mass for heterogeneous processes and calculations of gas-phase photolysis rates. Heterogeneous reactions considered in the model include those of N_2O_5, NO_3, NO_2, and HO_2 on wet aerosols, the uptake coefficients are taken to depend on atmospheric temperature and relative humidity, as described in *Liao and Seinfeld* [2005].

[8] The radiative effect of O_3 as well as that of internally mixed aerosols including sulfate, nitrate, ammonium, black carbon, and organic carbon are fed back into the GISS GCM. Aerosol optical properties (extinction cross section, single-scattering albedo, and asymmetry factor) are calculated by Mie theory based on wavelength-dependent refractive indices and aerosol size distributions. Assumptions and parameters used for the calculations of aerosol optical properties are given in *Liao et al.* [2004]. Water uptake by sulfate/nitrate/ammonium aerosols is determined by the aerosol thermodynamic equilibrium module, ISORROPIA [*Nenes et al.*, 1998]. Water uptake by organic carbon aerosol follows the treatment of *Chung and Seinfeld* [2002]. The refractive index of internally mixed aerosols is calculated by volume-weighting of the refractive index of each aerosol species and water. It should be noted that the actual (unknown) mixing state of aerosols in the atmosphere depends on the aging and coagulation of aerosol particles, and to some extent internal and external mixtures coexist. In our work the refractive index of the internal mixture is calculated by volume weighting as in most previous studies, but such a linear combination may represent an oversimplification. Present-day global optical depths and single-scattering albedos predicted by this model have been evaluated by comparison with measurements in *Liao et al.* [2004].

[9] In order to accentuate climate effects and feedbacks, we have selected IPCC scenario A2 [*Nakicenovic et al.*, 2000] for year 2100. Concentrations of CO_2, CH_4, N_2O, Chlorofluorocarbon (CFC)-11, CFC-12 are taken, respectively, to be 367 ppmv, 1760 ppbv, 316 ppbv, 246 pptv, and 535 pptv in present-day, and whereas 836 ppmv, 3731 ppbv, 447 ppbv, 45 pptv, and 222 pptv in year 2100. For simulations of O_3&AERs, present-day and year 2100 non-GHG anthropogenic emissions follow those in *Liao et al.* [2006] and the global and annual present-day and 2100 emissions of O_3 precursors, aerosols/aerosol precursors are given in Table 1. Biomass burning emissions are in part anthropogenic and in part natural. We assume in this study that the biomass burning emissions remain unchanged in 2000 and 2100; the effect of climate change on the occurrence and intensity of wildfires is not considered. The seasonal and geographical distributions of BC and POA emissions in year 2100 are obtained by scaling year 2000 monthly values, grid by grid, using projected changes in IPCC SRES A2 CO emissions. Climate-sensitive natural emissions, including lightning NO_x, NO_x from soil, biogenic hydrocarbons, and DMS, are calculated as described in *Liao et al.* [2006].

2.2. Experimental Design

[10] To examine the effect of chemistry-aerosol-climate coupling on prediction of future climate, and to identify the role of future climate change driven by GHGs and/or O_3&AERs themselves in predictions of future O_3&AERs, we present results of the following experiments:

[11] 1. CPLD2000: Equilibrium simulation of year 2000 O_3, aerosols, and climate with full chemistry-aerosol-climate coupling. The simulation is initialized at present-day GHG levels and with year 2000 non-GHG anthropogenic emissions for O_3 and aerosol chemistry. The GCM is integrated for 35 years, allowing O_3/aerosol levels to vary as the climate develops and using those varying levels in the radiative transfer calculation in the GCM.

[12] 2. CPLD2100: Equilibrium simulation of year 2100 O_3, aerosols, and climate with full chemistry-aerosol-climate coupling. This simulation is carried out in the same manner as CPLD2000 except that 2100 GHG concentrations and 2100 non-GHG emissions are used.

[13] 3. CHEM2100sw: Simulation of year 2100 O_3&AERs with present-day climate and year 2100 non-GHG anthropogenic emissions. This is the first of the two stepwise (sw) simulations for prediction of year 2100 climate; it provides offline fields of O_3&AERs for offline climate simulation CLIM2100sw (see below). The simulation is driven by the present-day climate saved from CPLD2000 (fixed climate) and run for 6 years using year 2100 non-GHG anthropogenic emissions. Averages of concentrations over the final 5 years are used to represent year 2100 O_3/aerosol distributions in present-day equilibrium climate that would occur if emissions were changed to 2100 levels.

[14] 4. CLIM2100sw: Equilibrium simulation of year 2100 climate using year 2100 levels of GHGs and monthly fields of year 2100 O_3&AERs from CHEM2100sw. This is the second of the two stepwise simulations for prediction of year 2100 climate. The chemistry modules in the unified model are turned off; only the GCM part of the model is used for this simulation. This equilibrium climate simulation is run for 35 years and meteorological fields averaged over the final 20 years are analyzed.

[15] 5. $CPLD2100_{GHG}$: Equilibrium simulation of year 2100 climate due to GHGs alone, and of O_3 and aerosol composition with that climate and 2100 emissions. This simulation is the same as CPLD2100, except that present-day monthly fields of O_3&AERs obtained from CPLD2000

			CPLD2000 **Coupling: O_3&AERs ◄► Climate** Climate: 2000 GHGs: 2000 concentrations O_3&AERs: 2000 emissions
Is 2100 climate considered in calculating 2100 O_3&AERs fields?	YES	$CPLD2100_{GHG}$ **Coupling: O_3&AERs ◄ Climate** Climate: 2100 GHGs: 2100 concentrations O_3&AERs: 2100 emissions	CPLD2100 **Coupling: O_3&AERs ◄► Climate** Climate: 2100 GHGs: 2100 concentrations O_3&AERs: 2100 emissions
	NO	CHEM2100sw **Coupling: none** Climate: 2000 from CPLD2000 O_3&AERs: 2100 emissions	CLIM2100sw **Coupling: O_3&AERs ► Climate** Climate: 2100 GHGs: 2100 concentrations O_3&AERs: 2100 concentrations from CHEM2100sw
		NO	YES
		Are O_3&AERs fields considered in GCM radiation code to calculate climate?	

Figure 1. Summary of numerical experiments. The comparison between CPLD2000 and CPLD2100 provides information about the expected change in climate and O_3 and aerosol fields between 2000 and 2100, based on the two-way coupling between O_3&AERs and climate. Comparisons between the four "2100" runs show the importance of coupling on future concentrations of O_3&AERs and climate.

are used in the radiative transfer code of the GCM during the integration, so that the GCM simulated climate is driven by future changes in GHGs alone. The simulation is initialized with GHGs set to 2100 levels and O_3&AERs to present-day fields in the radiative code of the GCM, while year 2100 non-GHG anthropogenic emissions are used for O_3 and aerosol chemistry. The model is integrated for 35 years, allowing O_3/aerosol levels to vary as the GHG-driven climate changes but these varying levels of O_3&AERs are not used in the radiative transfer calculation in the GCM. As a result, this simulation does not consider the effect of changing O_3&AERs on climate and therefore on concentrations of O_3&AERs themselves.

[16] The difference between CPLD2100 and CPLD2000 shows projected changes in O_3, aerosols, and climate from present-day to year 2100 with full chemistry-aerosol-climate coupling. The difference in climate between CPLD2100 and the stepwise simulation CLIM2100sw isolates the effect of chemistry-aerosol-climate coupling in future climate. The difference in concentrations of O_3&AERs between CPLD2100 and the stepwise simulation CHEM2100sw reflects the effect of coupling (mainly the effect of future climate change) on future concentrations of O_3&AERs. The role of GHG-driven climate change in predictions of future O_3&AERs can be assessed by differences in O_3&AERs between $CPLD2100_{GHG}$ and CHEM2100sw, whereas the role of climate change driven by O_3&AERs can be quantified by differences in O_3&AERs between CPLD2100 and $CPLD2100_{GHG}$. A summary of all the experiments is given in Figure 1. Concentrations of O_3&AERs averaged over the final 5 years of simulations and meteorological fields averaged over the final 20 years of climate simulations are presented in the following sections. Statistical analysis based on the student's two sample t-test is applied to the concentrations of the last 5 years and the meteorological fields of the last 20 years.

3. Predicted Changes in O_3, Aerosols, and Climate Over 2000–2100

[17] We present in this section results from comparing CPLD2100 and CPLD2000. GHG concentrations and non-GHG emissions change from their 2000 to their 2100 values, in a two-way coupled model: i.e. Climate impacts on O_3&AERs, and, in turn, O_3&AERs impact on climate.

3.1. Changes in Ozone Due to Changes in All Species

[18] Predicted changes in surface-layer mixing ratios and column burdens of O_3 over 2000–2100 as a result of the future changes in both climate and non-GHG anthropogenic emissions are shown in Figures 2a and 2b, respectively. Compared to the present-day O_3 levels, year 2100 surface-layer O_3 concentrations are predicted to generally increase by 40–100 ppbv over populated and biomass burning areas in January and July, and to decrease by up to 10 ppbv at Northern Hemisphere (NH) mid-high latitudes in July. Over 2000–2100, the global mean O_3 column burden is predicted to increase by 7.35 DU in DJF and by 9.70 DU in JJA. These values are lower than the global and annual increase of 11.4–20.5 DU simulated by 11 different chemical

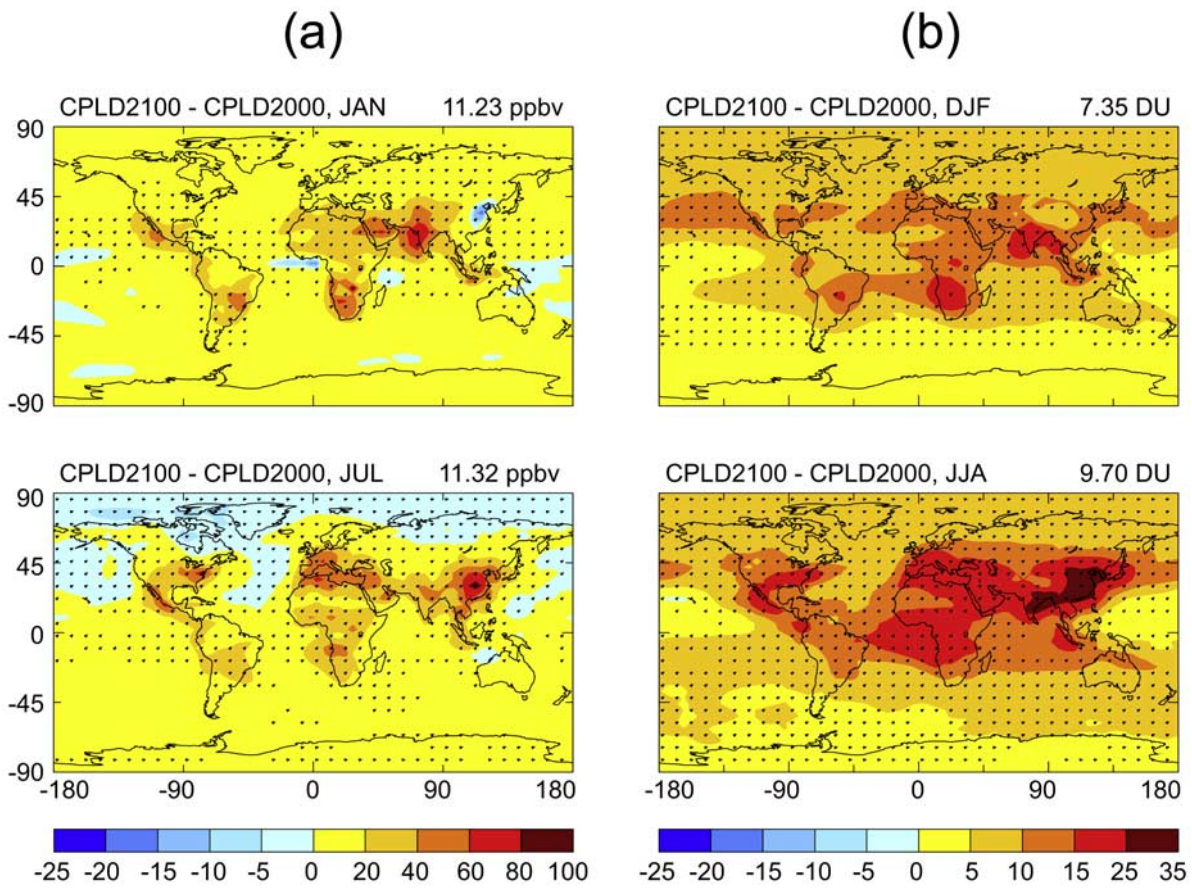

Figure 2. Predicted changes in O_3 over 2000–2100 (CPLD2100–CPLD2000) with full chemistry-aerosol-climate coupling for IPCC SRES A2. (a) Changes in surface-layer O_3 mixing ratios (ppbv) for January and July, and (b) changes in column burdens (DU) of O_3 for DJF and JJA (DJF = December–January–February, JJA = June–July–August). Global mean value is indicated at top right corner of each panel. Dotted areas indicate results that are significant at the 95% level.

transport models with changes in non-GHG anthropogenic emissions alone [*Gauss et al.*, 2003]. The differences are a result of future climate change, which will be discussed subsequently.

3.2. Changes in Aerosols Due to Changes in All Species

[19] Figure 3 shows projected changes in annual mean surface-layer concentrations and seasonal mean column burdens of different aerosol species over 2000–2100. On a global mean basis, all aerosol species, with the exception of sulfate, are predicted to increase between 2000 and 2100. (Anthropogenic emissions of sulfur decrease from present-day to 2100 in SRES A2.) Concentrations and burdens of organic carbon and nitrate aerosols are predicted to exhibit the largest growth over 2000–2100 in populated and biomass burning areas. Although mass changes of BC are relatively small as compared with those of organic carbon and nitrate, BC can have a disproportionate impact on climate because of its absorption. The bottom row of Figure 3 shows the predicted changes in surface concentrations and column burdens of total dry aerosol mass, the sum of sulfate, nitrate, ammonium, BC, POA, and SOA. Relative to the present-day aerosol concentrations and burdens, year 2100 values show reductions at high latitudes, because of the lower sulfate concentrations and predicted future increases in precipitation (increased wet deposition).

3.3. Climate Change Due to Changes in All Species, in GHGs, and in O_3&AERs

[20] Equilibrium climate change over 2000–2100 as a result of the changes in all species (GHGs and O_3&AERs) is represented by the differences in meteorological parameters between CPLD2100 and CPLD2000. For comparison, we also present simulated future climate change driven by GHGs alone (the differences between $CPLD2100_{GHG}$ and CPLD2000) and by O_3&AERs alone (CPLD2100-$CPLD2100_{GHG}$).

3.3.1. Temperature

[21] Figure 4 shows projected seasonal mean surface air temperature over 2000–2100 as a result of the changes in levels of all species, GHGs, and O_3&AERs. Relative to year 2000, year 2100 equilibrium global mean surface air temperature is predicted to increase by 6.1 K in DJF and by 5.8 K in JJA. In this version of GISS GCM II', doubling CO_2 relative to the present-day yields a climate sensitivity of 0.8 K m^2 W^{-1}, a value that lies within the range of sensitivities reported for current GCMs [*IPCC*, 2007]. Changes in surface air temperature are mostly the result of forcing by GHGs; the predicted global mean change by GHGs is +5.3 K in DJF and +5.0 K in JJA, while that by O_3&AERs is +0.82 K in DJF and +0.85 K in JJA. The net

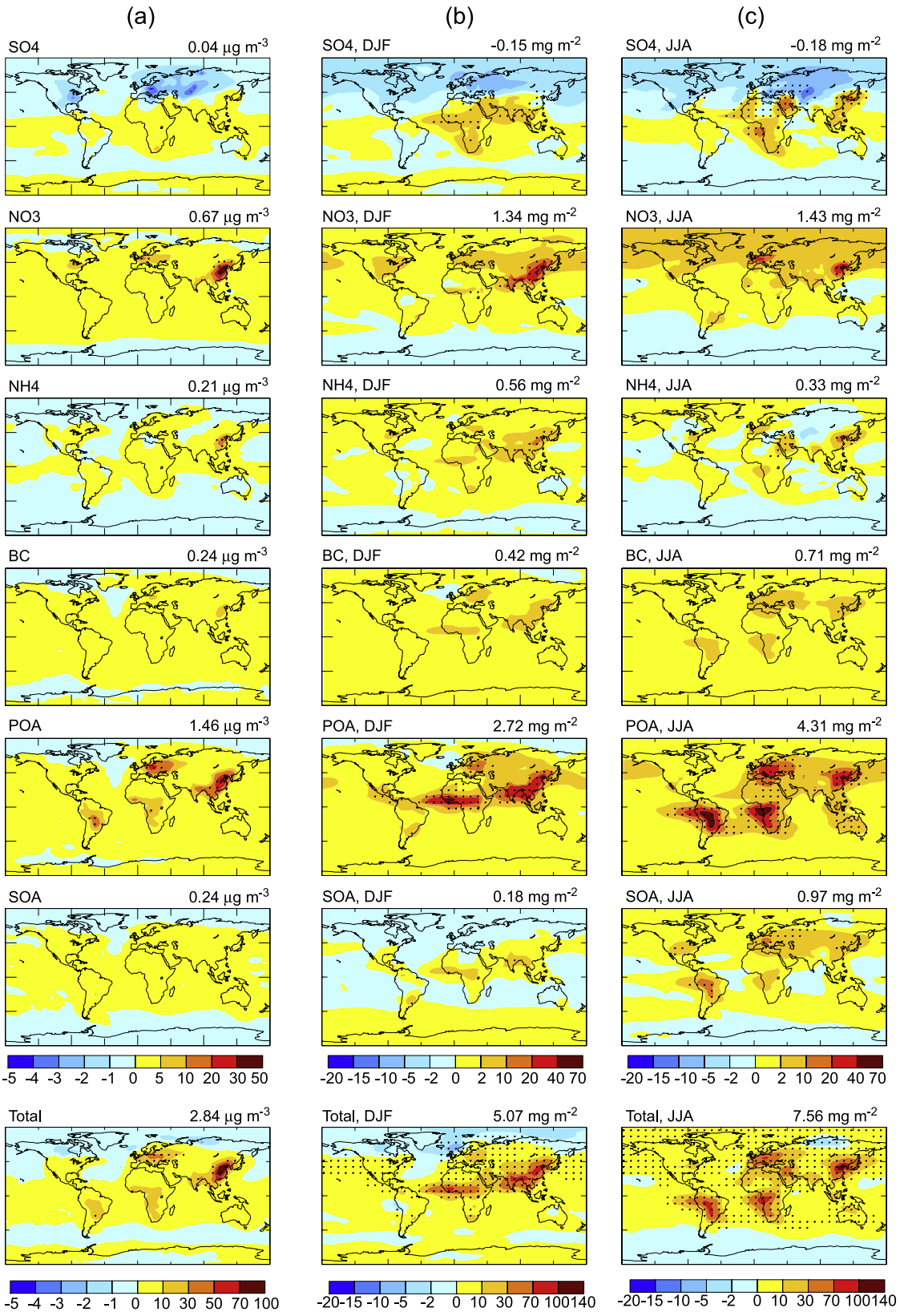

Figure 3. Predicted changes in aerosols over 2000–2100 (CPLD2100–CPLD2000) with full chemistry-aerosol-climate coupling for IPCC SRES A2. (a) Changes in annual mean surface-layer aerosol concentrations (μg m^{-3}). (b) and (c) are changes in aerosol column burdens (mg m^{-2}) for DJF and JJA, respectively. Aerosol species and global mean value are indicated for each panel. Total aerosol is the sum of SO_4^{2-}, NO_3^-, NH_4^+, BC, POA, and SOA. Dotted areas indicate results that are significant at the 95% level.

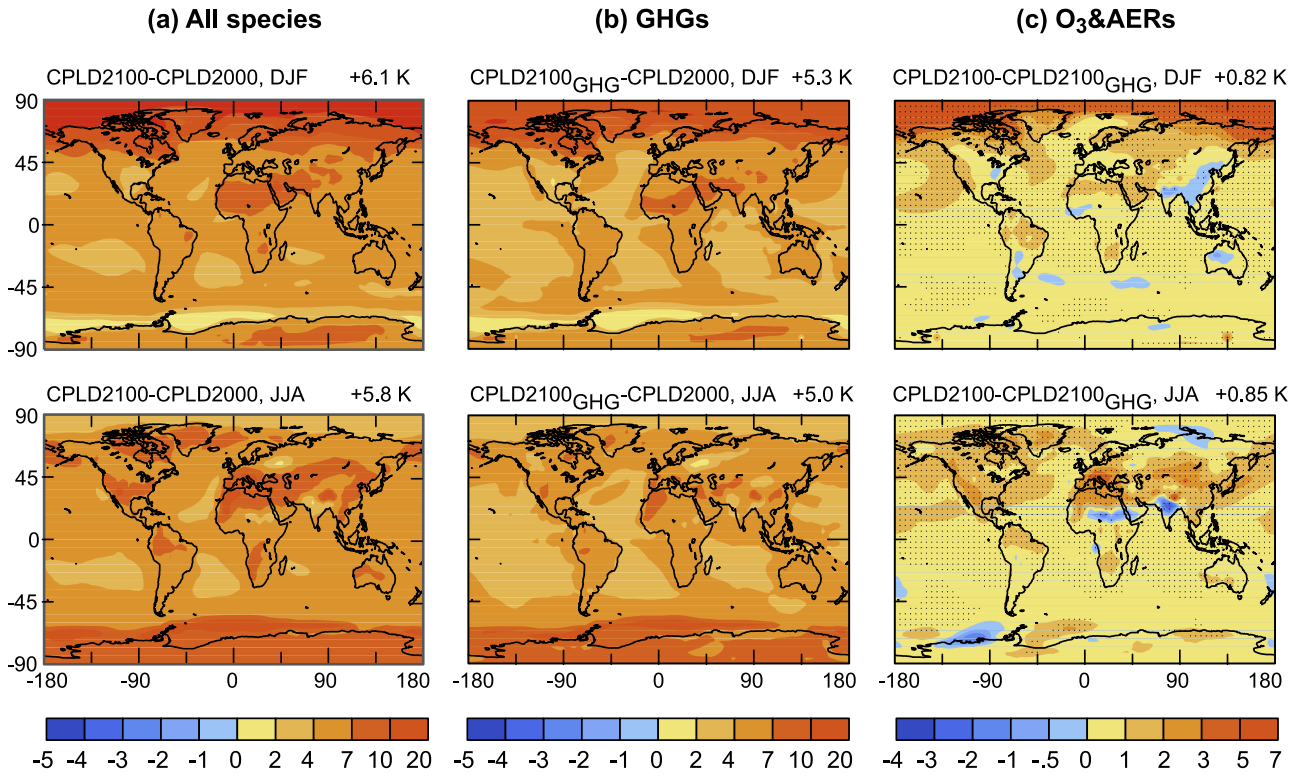

Figure 4. Equilibrium temperature responses (K) to the changes in (a) all species (GHGs, tropospheric ozone, and aerosols), (b) GHGs, and (c) O_3 and aerosols from present-day to year 2100 for IPCC SRES A2. Top row is for DJF and bottom row for JJA. Global mean value is indicated at top right corner of each panel. All colored areas in (a) and (b) and dotted areas in (c) are statistically significant at the 95% level, as determined by the student's two sample t-test. Note the color scale for (c) differs from the other two.

warming effect of O_3&AERs can be explained by the fact that the cooling effect of scattering aerosols is offset by warming owing to O_3 and the internally mixed BC containing aerosols.

[22] Predicted surface air temperature change by all species exhibits maximum increases over the high latitudes in the NH in DJF and in the Southern Hemisphere in JJA as a result of the snow and ice albedo feedback (Figure 4a). Such temperature response at high latitudes agrees with the predictions of forcing by both GHGs and short-lived species by *Levy et al.* [2008] and *Shindell et al.* [2008]. In JJA, a warming exceeding 7 K by all species is predicted over populated areas in eastern China, Europe, the United States, and in biomass burning areas in South America and Africa; besides the effect of GHGs (Figure 4b), a fraction of the warming is the result of short-lived species (Figure 4c). Because aerosols can reduce surface air temperature [*Chen et al.*, 2007] and O_3 is a greenhouse gas, the net effect of aerosols and O_3 is a weak, but statistically significant, cooling over eastern China in DJF, and over India and northern Africa in JJA (Figure 4c).

[23] Figure 5 displays the zonally averaged vertical distribution of predicted atmospheric temperature change over 2000–2100 by all species, GHGs, and O_3&AERs for DJF and JJA. With all species, predicted zonal mean changes in atmospheric temperature exhibit the same pattern as those summarized by *IPCC* [2007] (Figure 5a). Enhanced warming in both DJF and JJA in the tropical mid to upper troposphere results from enhanced latent heating owing to more vigorous moist convection [*Hansen et al.*, 1984; *Mitchell*, 1989] and from increased longwave radiative heating when upper tropospheric cloudiness and water vapor increase with temperature [*Dai et al.*, 2001]. The enhanced mid-tropospheric heating results mostly from future changes in GHGs (Figure 5b), which leads to a more stable lower troposphere in the low latitudes, a common feature in many GCMs [e.g., *Hansen et al.*, 1984; *Mitchell*, 1989; *Mitas and Clement*, 2006; *Chen et al.*, 2007]. Future changes in O_3&AERs are predicted to lead to additional mid-tropospheric heating in the low latitudes beyond the effect of GHGs alone (Figure 5c). In JJA, O_3&AERs have an effect of increasing atmospheric temperature in the NH, with the maximum heating predicted to be around 300 mb in the NH high latitudes, which is caused by O_3 and transported internally mixed absorbing aerosols [*Chung and Seinfeld*, 2005; *Chen et al.*, 2007]. The underlying high albedo surfaces in the NH high latitudes enhance the heating. On a zonal and seasonal mean basis, with larger increases in temperature in the upper troposphere versus in the lower troposphere, O_3&AERs increase atmospheric stability in the entire NH in JJA (Figure 5c).

3.3.2. Precipitation

[24] The predicted equilibrium precipitation changes as a result of changes in all species, GHGs, and O_3&AERs over 2000–2100 are presented for DJF and JJA in Figure 6. Predicted global mean changes in precipitation by all species are 0.34 mm day^{-1} for DJF and 0.31 mm day^{-1} for JJA, which are, respectively, 10% and 9% increases from the global mean values predicted for DJF and JJA in

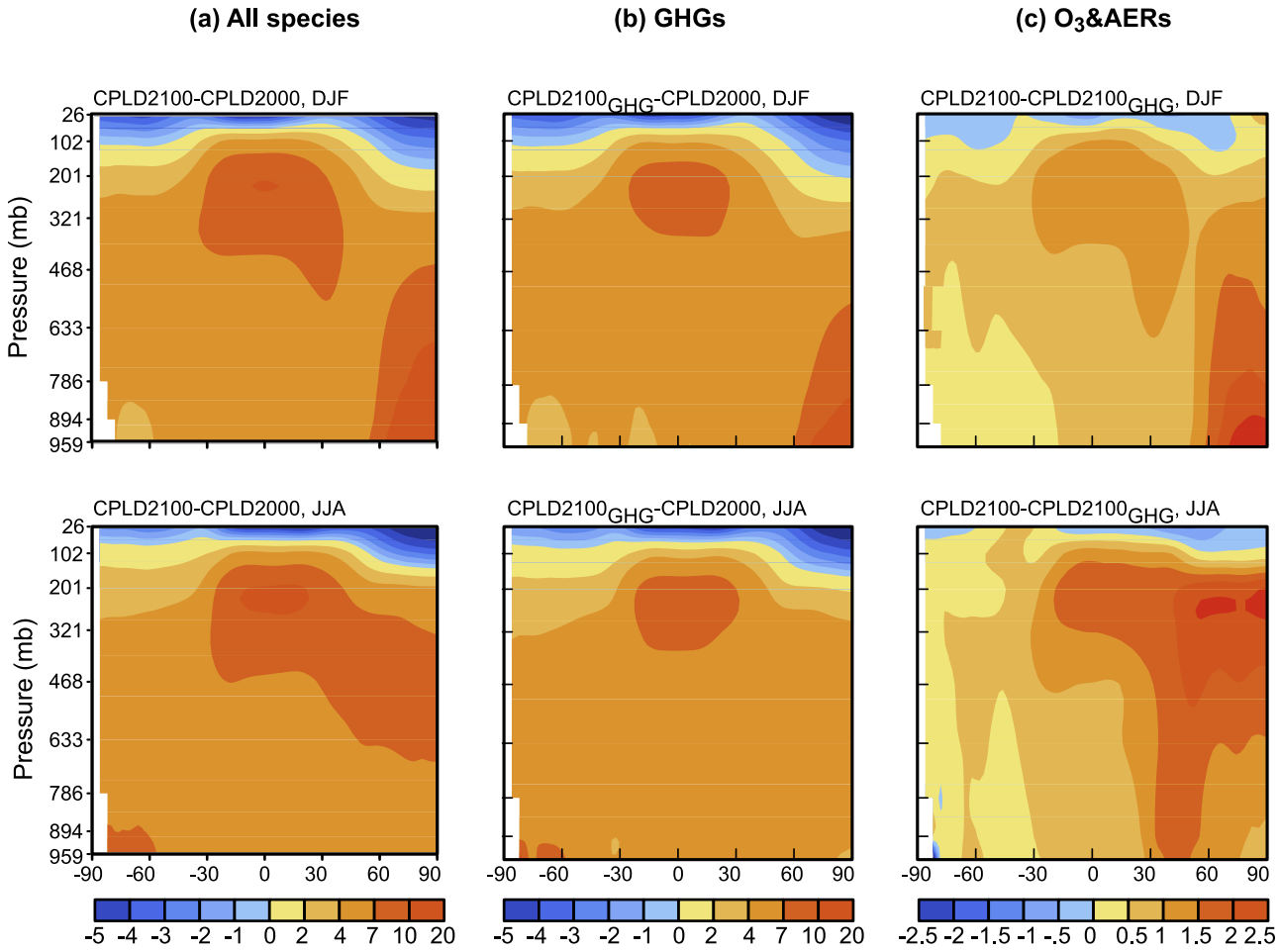

Figure 5. Equilibrium zonal and seasonal mean temperature responses (K) to the changes in (a) all species (GHGs, tropospheric ozone, and aerosols), (b) GHGs, and (c) O_3 and aerosols from present-day to year 2100 for IPCC SRES A2. Top row is for DJF and bottom row for JJA. All warming areas in (a) and (b) and all areas with warming of exceeding 0.5 K in (c) are statistically significant at the 95% level. Note color scale for (c) differs from the other two.

year 2000. Predicted increases in precipitation over mid to high latitudes in both hemispheres are a result of the large warming at the surface and in the lower troposphere [*Dai et al.*, 2001]; these results are consistent with those simulated using 23 different general circulation models [*Meehl et al.*, 2007]. In the presence of forcing by all species, precipitation is predicted to decrease over southeastern China, South Asia, northern and southern Africa in DJF and over eastern China, Europe, the United States, South America, and southern Africa in JJA. The net effect of O_3&AERs generally leads to reductions in precipitation over populated areas (Figure 6c), with the reductions statistically significant over eastern China in both DJF and JJA and over Europe in JJA, since aerosols lead to reduced convection [*Chen et al.*, 2007].

4. Importance of Chemistry-Aerosol-Climate Coupling

[25] In this section we systematically examine the importance of considering two-way, one-way, or no couplings between O_3&AERs and climate on the calculated O_3 and aerosol burdens and climate. We do so by performing two comparisons of the two-way (O_3&AERs⇒climate) coupled simulation, CPLD2100: (1) with CHEM2100sw, in which no couplings between O_3&AERs and climate are considered; (2) with CLIM2100sw, in which the one-way (O_3&AERs⇒climate, O_3&AERs influence climate through their radiative forcing) coupling is allowed.

4.1. Two-Way Coupling (O_3&AERs ⟺ Climate) vs. No Coupling: Effect on O_3 and Aerosols

4.1.1. Ozone

[26] The effect of climate change on future levels of O_3 can be seen from the differences in column burdens of O_3 between CPLD2100 and CHEM2100sw (Figure 7a). Relative to CHEM2100sw (year 2100 O_3 using present-day climate and year 2100 non-GHG emissions), CPLD2100 predicts lower column burdens of O_3 with fully-coupled climate change. The simulated global mean column burden of O_3 in DJF in CPLD2100 is 6 DU (or 21% lower) than the 29 DU simulated in CHEM2100sw, while that in JJA in CPLD2100 is 8 DU (or 17%) lower than the 48 DU in CHEM2100sw. The increases in temperature (Figure 4) and the associated increases in water vapor content in a warmer

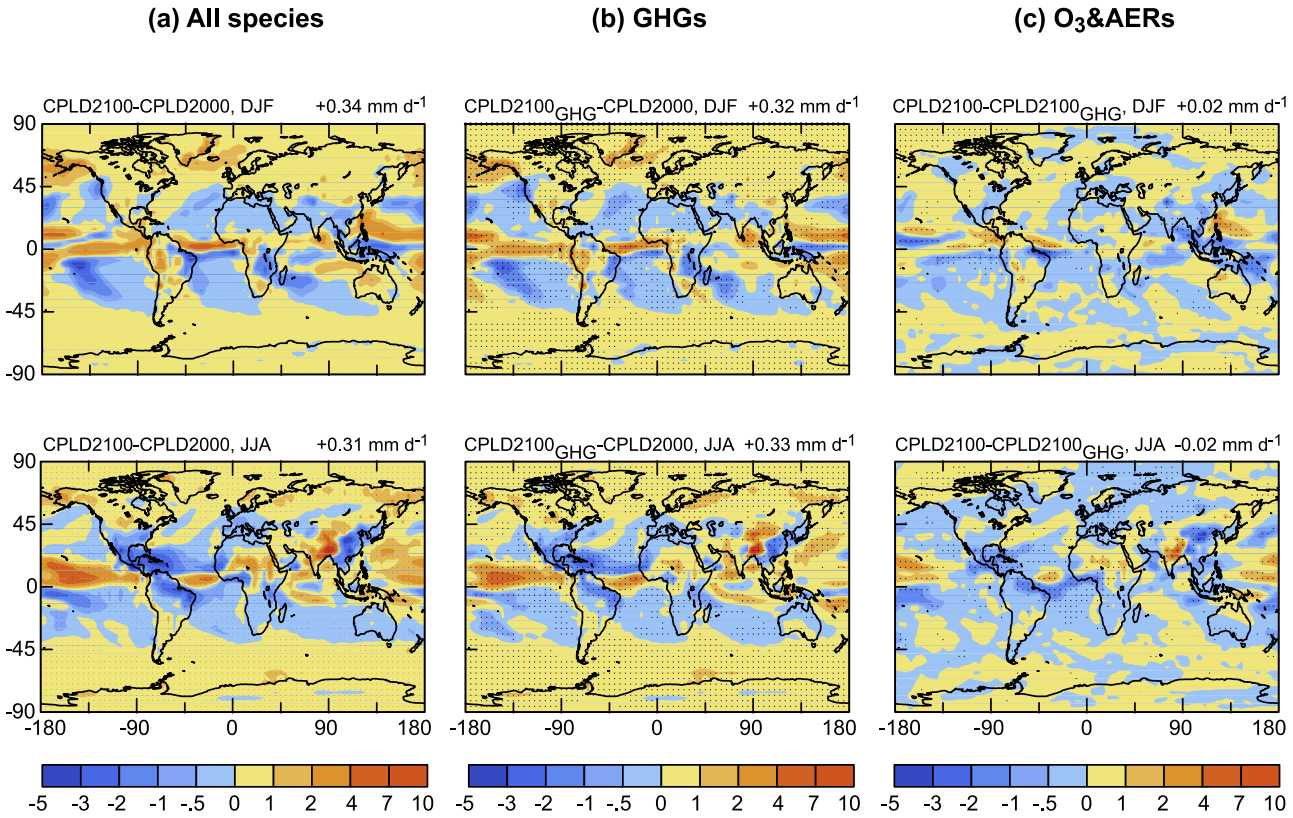

Figure 6. Predicted responses in seasonal mean equilibrium precipitation (mm day^{-1}) by changes in (a) all species, (b) GHGs, and (c) O_3 and aerosols over 2000–2100 for IPCC SRES A2. Upper panels are for DJF and bottom panels for JJA. Global mean value is indicated at the top right corner of each panel. Dotted areas indicate results that are significant at the 95% level.

climate lead to faster removal of O_3 in the troposphere [*Brasseur et al.*, 1998; *Johnson et al.*, 1999, 2001; *Stevenson et al.*, 2006]. The largest differences in O_3 column burden are predicted to be 10–20 DU in DJF and 15–25 DU in JJA over tropics and subtropics (Figure 7a) where water vapor content is predicted to exhibit the largest increases over 2000–2100 [*Chen et al.*, 2007]. With full chemistry-aerosol-climate coupling in CPLD2100, year 2100 column burdens of O_3 over eastern China, the United States, and Europe, respectively, are predicted to be lower than those simulated in CHEM2100sw by 10–25%, 10–15%, and 5–10% in DJF, and by 5–10%, 5–15%, and 0–5% in JJA. The zonal mean differences in O_3 mixing ratios between CPLD2100 and CHEM2100sw are shown in Figure 7b for January and July. Ozone differences are predicted to exceed 20 ppbv near the tropopause where O_3 mixing ratios are high in CHEM2100sw.

4.1.2. Carbonaceous Aerosols

[27] Figure 8 shows the effect of climate change (CPLD2100 - CHEM2100sw) on column burdens of BC, POA, and SOA for DJF and JJA. Predicted changes in column burdens of BC are similar to those of POA in both DJF and JJA. Relative to CHEM2100sw, POA burdens simulated in CPLD2100 are predicted to be lower in mid to high latitudes in both hemispheres because of the predicted increases in precipitation in these areas over 2000–2100 (Figure 6a). Relative to CHEM2100sw, year 2100 JJA POA burdens over northeastern China, Europe, southern Africa, and South America, however, are predicted to increase by 10–35 mg m^{-2} as a result of fully coupled climate change. Aerosols, which are predicted to lead to reduced precipitation (Figure 6c), exert a positive feedback to further increase aerosol concentrations over areas with high levels of aerosols.

[28] The pattern of changes in SOA column burden is similar to that of changes in POA, since SOA is assumed to form on preexisting POA [*Liao et al.*, 2003]. Although higher temperatures in CPLD2100 lead to a 92% increase in simulated year 2100 emissions of monoterpenes and ORVOCs as compared CHEM2100sw, the higher temperatures serve to shift the gas-particle partitioning of volatile oxidation products toward the gas-phase. The net effect of these two opposing influences as well as the changes in precipitation is a 13% higher global SOA burden in CPLD2100 than in CHEM2100sw (Table 2).

4.1.3. Sulfate/Nitrate/Ammonium

[29] Figure 9 shows the effect of full coupling (CPLD2100 - CHEM2100sw) on column burdens of sulfate, nitrate, and ammonium for DJF and JJA. The largest increases in sulfate column burden are predicted over southeastern Asia and the south Asia subcontinent. In JJA, simulated column burdens of sulfate in CPLD2100 are 5–35 mg m^{-2} higher than those in CHEM2100sw over eastern China, Europe, the Arabian Peninsula, eastern United States, and Africa. In addition to the differences in meteorological conditions between CPLD2100 and

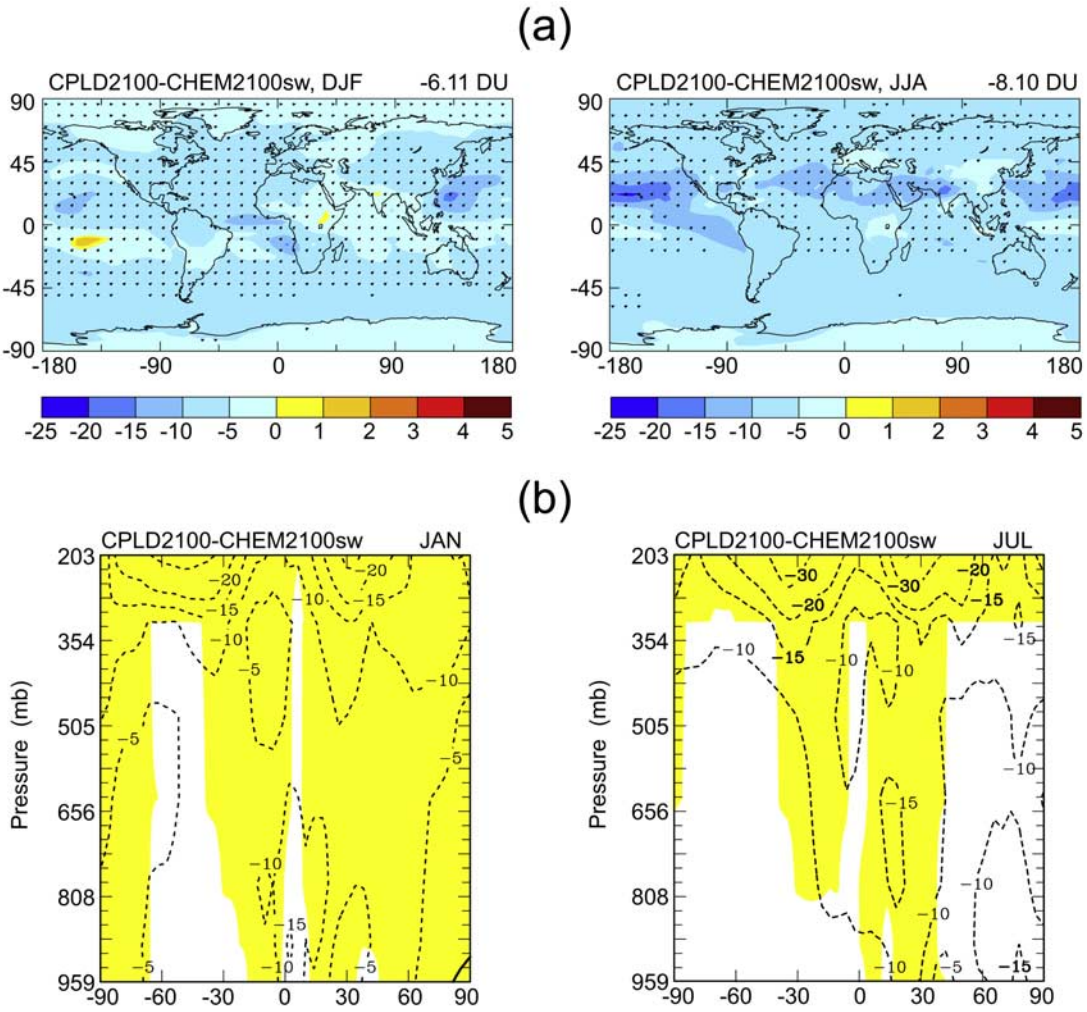

Figure 7. (a) Effect of chemistry-aerosol-climate coupling on year 2100 column burdens (DU) of O_3 (CPLD2100−CHEM2100sw) for DJF and JJA for IPCC SRES A2. (b) Differences in year 2100 zonal mean O_3 mixing ratios (ppbv) between CPLD2100 and CHEM2100sw for the months of January and July. Global mean value is indicated at top right corner of each panel for (a). Dotted areas in (a) and yellow areas in (b) indicate results that are significant at the 95% level.

CHEM2100sw, locally higher O_3, OH, and H_2O_2 concentrations in a warmer climate lead to increased sulfate formation near emission sources. Although climate change is predicted to generally lead to reduced column burdens of O_3 (Figure 7), JJA surface-layer O_3 is predicted to increase over populated areas and biomass burning regions (see, for example, Figure 15b that shows the effect of future climate change on surface O_3 for the month of July). Concentrations of OH and H_2O_2 increase over populated areas in JJA (not shown) as a result of climate change, with the increases in OH associated with the increases in O_3 and those in H_2O_2 explained by the increased rate coefficient of the reaction $HO_2 + HO_2 \rightarrow H_2O_2$ in a warmer climate [*Liao et al.*, 2006]. The role of climate-induced changes in oxidants can also be identified over the eastern United States, where, relative to CHEM2100sw, column burdens of sulfate increase but those of chemically inert POA and BC do not show significant changes.

[30] Changes in temperature influence gas-aerosol thermodynamic equilibrium. In a warmer climate, more HNO_3 remains in the gas-phase, leading to significant reductions in ammonium nitrate formation. Relative to CHEM2100sw, column burdens of nitrate and ammonium in the fully coupled CPLD2100 are generally lower, although the burdens show minor increases over northeastern China and Europe as a result of the reduced precipitation in those locations. On an annual mean basis, global burdens of nitrate and ammonium aerosols are 44% and 25% lower, respectively, in CPLD2100 than in CHEM2100sw (Table 2).

4.1.4. Total Aerosols

[31] The differences in total aerosol column burden, including sulfate, nitrate, ammonium, BC, POA, and SOA, between CPLD2100 and CHEM2100sw are shown in Figure 10a. In mid to high latitudes in the NH, the full coupling (the effect of climate change) leads to reductions in aerosol column burden of 10–20 mg m^{-2} (or 40–80%) in DJF and of up to 10 mg m^{-2} (or 20–40%) in JJA, as compared with the values obtained in the stepwise simulation CHEM2100sw. Relative to CHEM2100sw, total aerosol column burdens predicted in CPLD2100 are lower by up to 20 mg m^{-2} over the eastern United States, northeastern China, and Europe in

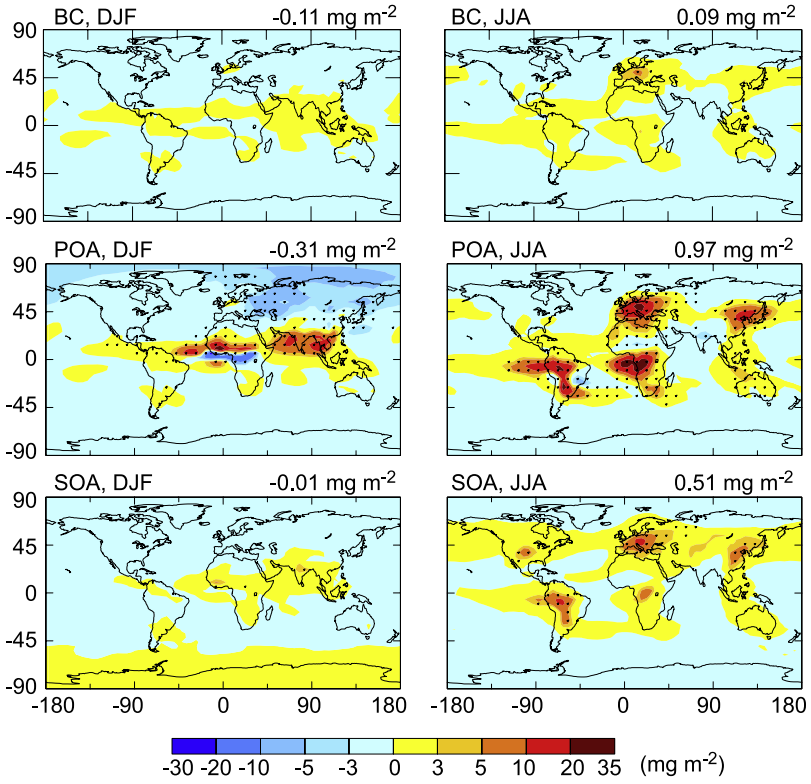

Figure 8. Effect of chemistry-aerosol-climate coupling on year 2100 column burdens (mg m^{-2}) of black carbon (BC), primary organic carbon (POA), and secondary organic aerosol (SOA) in DJF and JJA for IPCC SRES A2. Results shown are differences between CPLD2100 and CHEM2100sw (CPLD2100−CHEM2100sw). Global mean value is indicated at the top right corner of each panel. Dotted areas indicate results that are significant at the 95% level.

DJF, while burdens are higher by 30–50 mg m^{-2} over populated and biomass burning areas in JJA.

[32] The effect of full coupling on simulated year 2100 zonal mean total aerosol mass concentrations is shown for DJF and JJA in Figure 10b. Compared to CHEM2100sw, aerosol concentrations in CPLD2100 are lower at high latitudes in the NH in DJF, with the largest reductions predicted near the surface. By contrast, aerosol concentrations are predicted to increase over the tropics and subtropics in both DJF and JJA; the increases are mainly below 600 mb altitude because of the future increases in atmospheric stability in the lower troposphere as a result of the enhanced mid-tropospheric heating (Figure 5a). It should be noted here that the effects of climate change on aerosols include not only the changes in meteorological parameters but also changes in climate-sensitive emissions, especially dimethylsulfide (DMS) emissions over the oceans and biogenic emissions over continents.

4.2. Two-Way Coupling (O_3&AERs ⟺ Climate) vs. One-Way Coupling (O_3&AERs⇒Climate): Effect on Climate

4.2.1. Changes in Radiative Fluxes Associated With Differences in O_3 and Aerosols

[33] CLIM2100sw is an equilibrium simulation using 2100 GHG levels and offline monthly ozone and aerosol fields from CHEM2100sw; climate is not allowed to impact on the O_3 and aerosol fields, but O_3 and aerosol fields impact on climate through their direct radiative forcing (O_3&AERs⇒climate one-way coupling). The differences in O_3 and aerosol burdens used in CLIM2100sw (i.e. fixed offline fields from CHEM2100sw) and those simulated in CPLD2100 can produce a difference in net radiative fluxes, leading to the difference in climate between CLIM2100sw and CPLD2100. By carrying out offline radiative calculations, these changes in radiative fluxes are analyzed

Table 2. Predicted Annual Mean Global Burdens (Tg) of O_3 and Aerosols in CHEM2100sw and CPLD2100, as well as Predicted Global Annual Mean Surface Air Temperature and Precipitation in CLIM2100sw and CPLD2100

Predicted Year 2100 Global Burden (Tg)		
Species	CHEM2100sw	CPLD2100
O_3	511.7	433.7
SO_4^{2-}	1.91	1.91
NO_3^-	2.06	1.16
NH_4^+	1.09	0.82
BC	0.52	0.50
POA	2.90	2.94
SOA	0.53	0.60
All aerosol	9.01	7.93
Predicted Year 2100 Global Mean Meteorological Parameters		
	CLIM2100sw	CPLD2100
Surface air temperature (°C)	20.70	21.12
Precipitation (mm day^{-1})	3.65	3.68

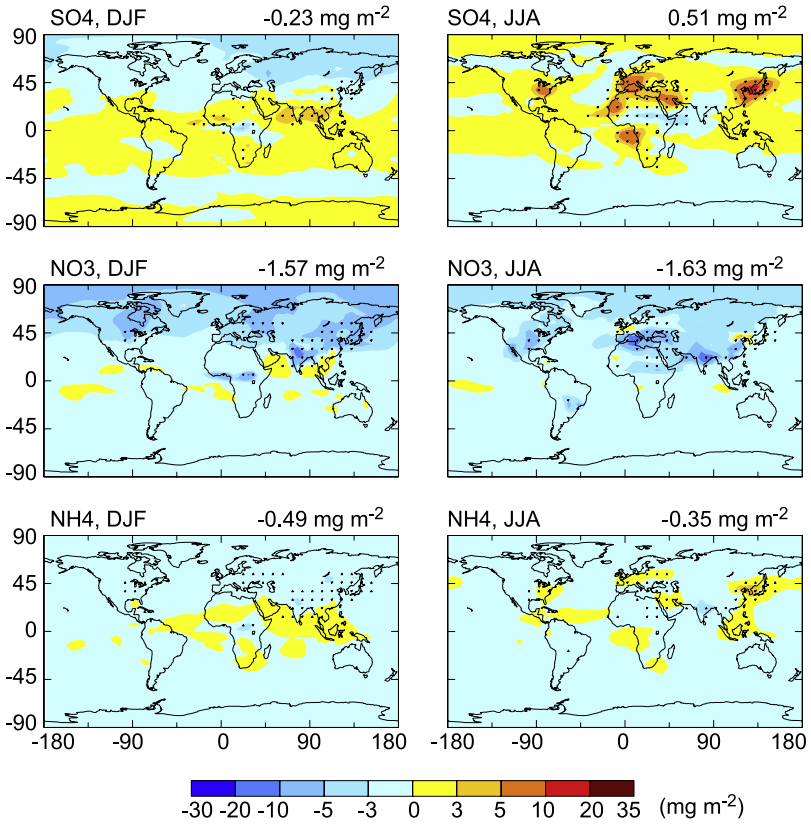

Figure 9. Effect of chemistry-aerosol-climate coupling (CPLD2100−CHEM2100sw) on year 2100 column burdens (mg m^{-2}) of sulfate (SO_4^{2-}), nitrate (NO_3^-), and ammonium (NH_4^+) aerosols for DJF and JJA for IPCC SRES A2. Global mean value is indicated at the top right corner of each panel. Dotted areas indicate results that are significant at the 95% level.

in this section to investigate the radiation perturbations between the two-way coupled simulation CPLD2100 and the one-way (O_3&AERs⇒climate) coupled simulation CLIM2100sw.

[34] Figure 11 shows the O_3 radiative perturbation to CLIM2100sw at the tropopause and the surface as a result of two-way coupling. Since O_3 column burdens in CPLD2100 are generally lower than those in CLIM2100sw (Figure 7), an overall cooling is found at the tropopause in both DJF and JJA. At the surface, increases in shortwave heating and reductions in longwave heating lead to modest net heating (shortwave plus longwave) in the summer hemisphere and net cooling in mid-high latitudes in the winter hemisphere. Regionally, O_3 forcing values are within the range of ±1.5 W m^{-2} at both the tropopause and the surface.

[35] Figure 12 presents the aerosol radiation perturbation as a result of two-way coupling at different vertical layers. The magnitude of aerosol radiation perturbation is generally larger than that of O_3. In DJF, over mid-high latitudes in both hemispheres, reductions in aerosols owing to two-way coupling generally lead to a positive increase in net radiative fluxes in the lower troposphere, with maximum values of 2−5 W m^{-2} extending from the Mediterranean Sea to Eastern Europe and eastern Asia. Although DJF column burdens of all aerosols over eastern China and Europe are lower with two-way coupling (Figure 10a), concentrations of aerosols in the lower troposphere are actually higher (Figure 16b), leading to increases in backscattering and hence negative forcing in the upper troposphere of these areas. In JJA, aerosol radiation perturbation in the lower and upper troposphere has generally an opposite sign; over areas where two-way coupling leads to lower aerosol burdens (Figure 10a), aerosol radiation perturbation is positive in the lower troposphere and negative in the upper troposphere; over populated areas where two-way coupling leads to higher aerosol burdens, radiation perturbation is negative in the lower troposphere and positive in the upper troposphere. Over the tropics, negative changes of 10−15 W m^{-2} are found in the lower troposphere and ±2 W m^{-2} are estimated in the upper troposphere in both DJF and JJA, as a result of the higher levels of aerosols owing to two-way coupling.

4.2.2. Surface Air Temperature

[36] Figure 13 shows the differences in simulated surface air temperature between two-way coupling (CPLD2100) and one-way O_3&AERs⇒climate coupling (CLIM2100sw) for DJF and JJA. The effect of two-way coupling produces stronger warming by O_3&AERs; global mean year 2100 surface air temperature simulated in CPLD2100 is higher than that obtained in CLIM2100sw by 0.44 K in DJF and by 0.41 K in JJA.

[37] Comparison of Figure 13 with Figure 12 indicates that the geographical pattern of the surface air temperature response does not always follow that of direct radiative forcing, which has been demonstrated in earlier studies [*Hansen et al.*, 1997; *Mickley et al.*, 2004; *Chung and Seinfeld*, 2005]. In DJF, surface air temperatures simulated

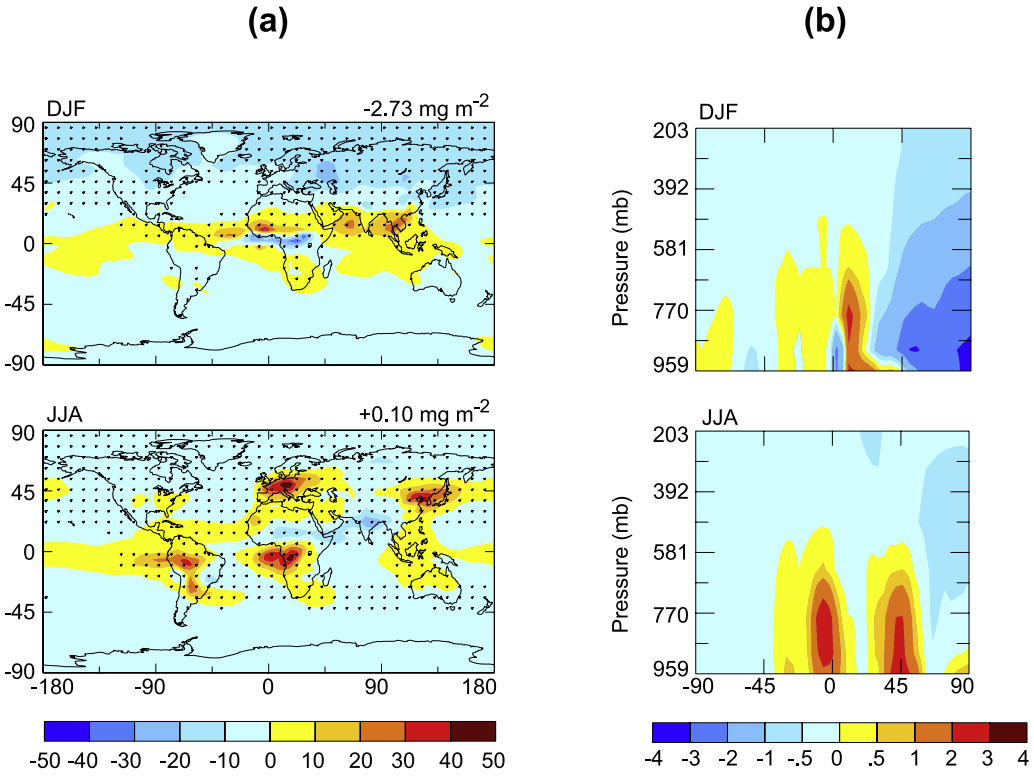

Figure 10. (a) Effect of chemistry-aerosol-climate coupling on year 2100 column burdens (mg m^{-2}) of all aerosols (CPLD2100−CHEM2100sw) for DJF and JJA. (b) Differences in year 2100 zonal and seasonal (DJF or JJA) mean total aerosol concentrations (μg m^{-3}) between CPLD2100 and CHEM2100sw. Aerosol species accounted for are sulfate, nitrate, ammonium, BC, POA, and SOA. Global mean value is indicated at top right corner of each panel for (a). Dotted areas indicate results that are significant at the 95% level.

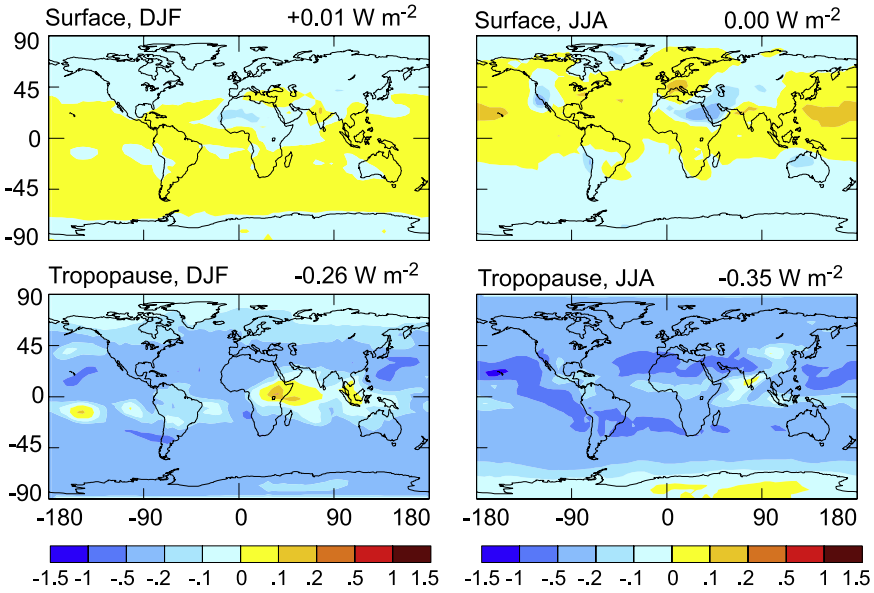

Figure 11. Changes in radiative fluxes (W m^{-2}) at the surface and the tropopause as a result of the differences in O_3 between two-way coupling (CPLD2100) and one-way O_3&AERs⇒climate coupling (CLIM2100sw). Left column is for DJF, and right column for JJA. Global mean value is indicated at the top right corner of each panel.

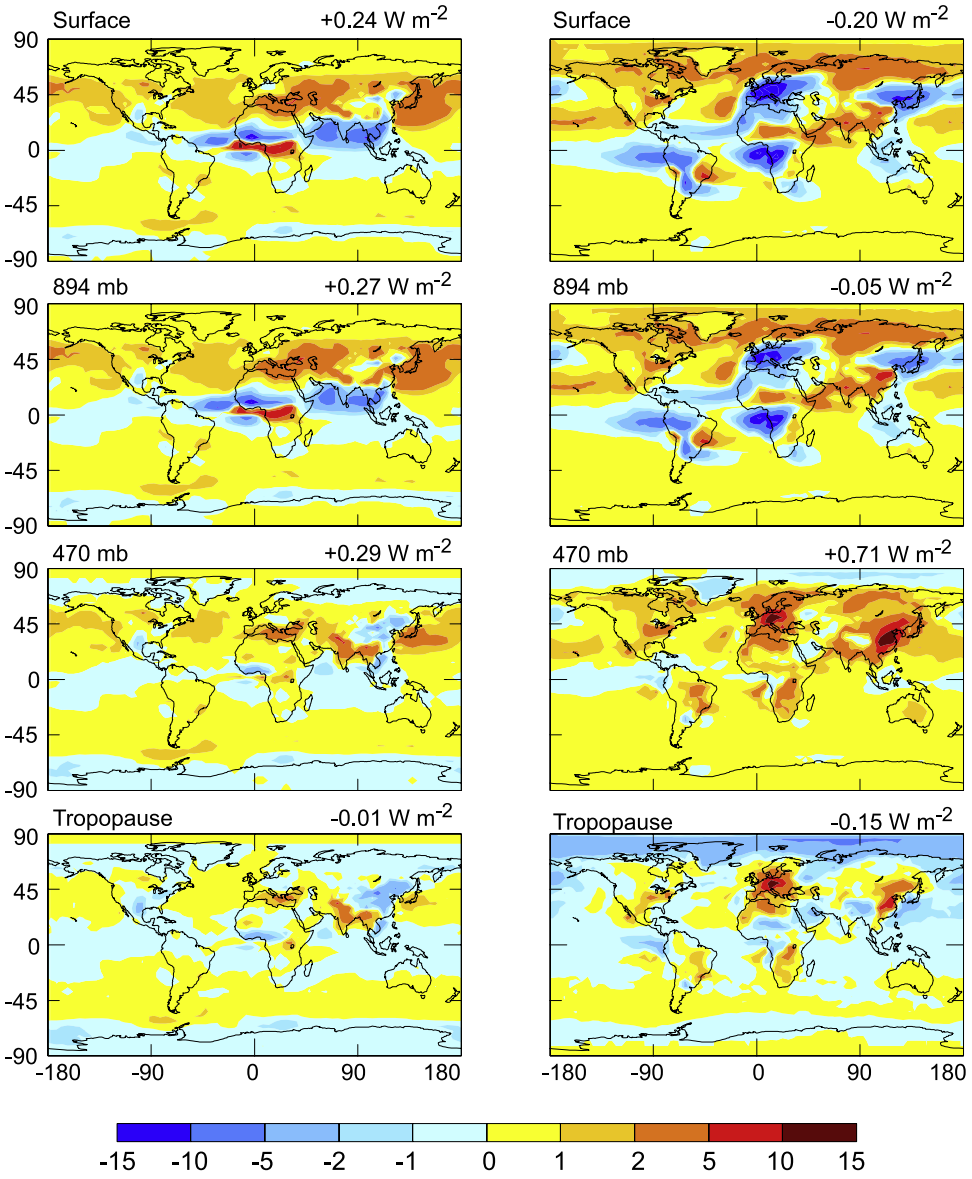

Figure 12. Changes in radiative fluxes (W m^{-2}) at the surface, 894 mb, 470 mb, and the tropopause as a result of the differences in aerosols (sulfate, nitrate, ammonium, BC, POA, and SOA) between two-way coupling (CPLD2100) and one-way O_3&AERs⇒climate coupling (CLIM2100sw). (a) DJF and (b) JJA. Global mean value is indicated at the top right corner of each panel.

in CPLD2100 are higher than those from CLIM2100sw at mid-high latitudes in the NH, corresponding to the positive forcing in the lower troposphere. While the maximum positive forcing values are in the NH mid-latitudes, the maximum changes in surface air temperature of 2–4 K are predicted in NH high latitudes as a result of the sea-ice climate feedback. Statistically significant higher DJF temperatures of 1–2 K in CPLD2100 than in CLIM2100sw over Europe correspond to the large positive forcing there. The surface temperature in CPLD2100 is higher than that in CLIM2100sw by 1–2 K in eastern China in DJF, and this statistically significant warming extends to India and southeastern Asia. These changes in temperature in Asia do not correspond with the location of forcing; since the positive forcing is small or near zero over eastern China and negative over India and southeastern Asia. In JJA, although negative forcings are large in the lower troposphere over populated and biomass burning areas (Figure 12), differences in JJA surface air temperature (CPLD2100-CLIM2100sw) do not show statistically significant cooling in these areas, because the less stable atmospheric lapse rate in JJA than in DJF tends not to confine the thermal response close to the surface. Statistically significant increases in JJA surface air temperature of 1–2 K are predicted over Europe, despite the negative forcing there in the lower troposphere, which is probably influenced by the warming in the nearby ocean and in higher latitudes. Statistically significant increases in surface air temperature are also found over the northwestern Pacific Ocean, tropical Pacific Ocean, and northern Indian Ocean. Increases in black carbon aerosols over populated areas can contribute to the positive temperature responses over tropical oceans [*Chung and Seinfeld*, 2005].

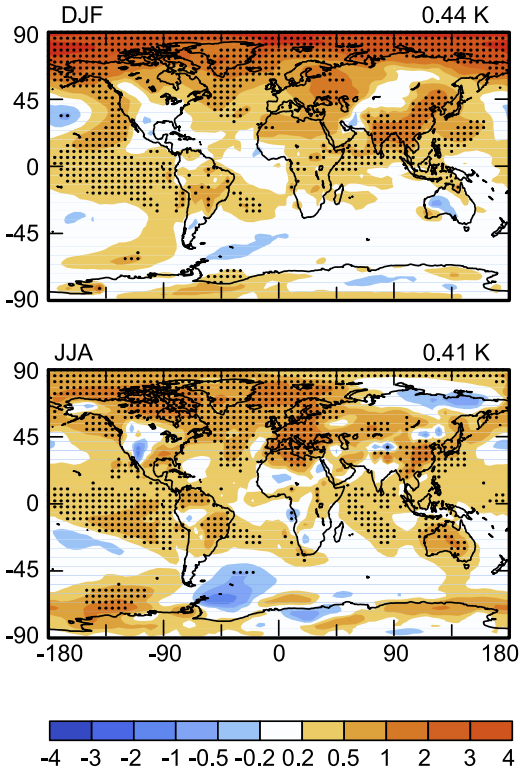

Figure 13. Effect of chemistry-aerosol-climate coupling on year 2100 seasonal mean surface air temperature (K). Results shown are the differences in temperature between CPLD2100 and CLIM2100sw (CPLD2100–CLIM2100sw). Global mean value is indicated at top right corner of each panel. Dotted areas indicate results that are significant at the 95% level.

[38] The importance of chemistry-aerosol-climate coupling in prediction of future surface air temperature change can be represented by the ratios of the difference in temperature between CPLD2100 and CLIM2100sw (Figure 13) to that between CPLD2100 and CPLD2000 (Figure 4a), which are about 10–30% in the North Polar Region, 20–40% in DJF and 10–20% in JJA over eastern China, as well as 10–30% in Europe in both seasons. These results indicate that the effect of coupling is important regionally in predictions of decadal temperature changes.

4.2.3. Precipitation

[39] Figure 14 shows the differences in simulated precipitation between CPLD2100 and CLIM2100sw for DJF and JJA. The largest differences in predicted precipitation generally overlap or are near the regions with the largest temperature differences such as high latitudes in the NH, eastern China, and tropical oceans. As shown in the zonal mean plot (Figure 14b), the full coupling (CPLD2100-CLIM2100sw) influences mainly precipitation between 20°S and 20°N, and produces increased precipitation in mid-high latitudes in the NH in both DJF and JJA.

5. Contribution of Changes in GHG- and O_3&AERs to Year 2100 O_3 and Aerosols

[40] As presented in section 4, the differences in O_3 (or aerosols) between CPLD2100 and CHEM2100sw represent the effect of the two-way (O_3&AERs $\Longleftrightarrow$ climate) coupling on simulation of future O_3 (or aerosols). Future climate in CPLD2100 includes the effects of future changes in both GHGs and O_3&AERs; we quantify in this section the relative importance of future GHG- and O_3&AERs-driven climate change on levels of year 2100 O_3&AERs themselves. The differences in simulated concentrations of O_3&AERs between $CPLD2100_{GHG}$ and CHEM2100sw represent the effect of future climate change driven by GHGs, while those between CPLD2100 and $CPLD2100_{GHG}$ assess the effect of future climate change driven by O_3&AERs. Because of the intricate coupling between O_3 and aerosols, it is not possible to separate the climate impact of O_3 from that of aerosols. Aerosols exert a greater climate forcing than O_3 [*Chen et al.*, 2007]; that is, future climate change by O_3&AERs is dominated by the aerosol component.

5.1. Ozone

[41] Figure 15a shows year 2100 surface-layer O_3 mixing ratios predicted in CPLD2100. Future concentrations of O_3, based on IPCC SRES A2 that has the highest growth of emissions among the IPCC scenarios, are all at the high end. Figures 15b–15d compare impacts of future climate change by all species (GHGs plus O_3&AERs) (CPLD2100-CHEM2100sw), GHGs ($CPLD2100_{GHG}$-CHEM2100sw), and O_3&AERs (CPLD2100 - $CPLD2100_{GHG}$) on predicted year 2100 surface-layer O_3 mixing ratios for January and July. Relative to CHEM2100sw simulated with present-day climate, surface O_3 in CPLD2100 generally increases over populated and biomass burning areas as a result of future climate change by all species (Figure 15b). Future climate change by GHGs (Figure 15c) increases surface layer O_3 concentrations over or near populated and biomass burning areas because of slower transport, enhanced biogenic hydrocarbon emissions, decomposition of peroxyacetyl nitrate at higher temperatures, and the increase of O_3 production by increased water vapor at high NO_x levels [*Liao et al.*, 2006]. Because the net effect of O_3&AERs on temperature is to increase atmospheric stability (reductions in convection) in JJA (see section 3.3.1 for zonal mean changes in atmospheric stability and Table 4 in *Chen et al.*, 2007 for changes in stability over populated areas), O_3 concentrations over eastern China, eastern US, and Europe are predicted to increase in JJA when photochemistry is active (Figure 15d). The maximum increases in O_3 of 20–30 ppb are predicted over Europe in July, because Europe is an area with strong moist convection in the GISS GCM [*Rind et al.*, 2001], therefore reductions in convection there have large impact on O_3. This predicted increase in O_3 in July over Europe is a robust result in this model, since the predicted increase in atmospheric stability there in JJA is statistically significant. Future climate change driven by GHGs has a considerably larger impact on future O_3 than that driven by O_3&AERs. For example, comparison of Figures 15b and 15c indicates that 85% of the global mean reduction in O_3 in January (6.79 ppbv) and 81% of the global mean reduction in July (7.76 ppbv) are attributable to future GHG-driven climate. Over eastern China, eastern United States, and biomass burning areas of Southern Africa and South America, increases in O_3 by future GHG-driven climate account for more than 80% of the increases by future climate change by all species.

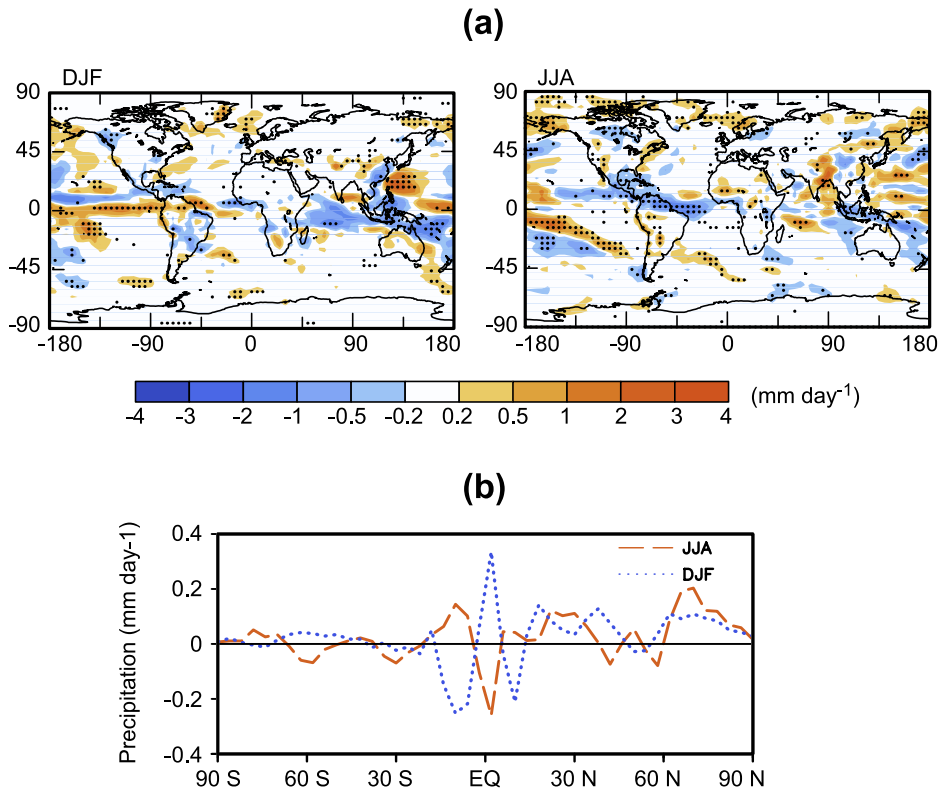

Figure 14. Effect of chemistry-aerosol-climate coupling on year 2100 seasonal mean (a) precipitation (mm day^{-1}) and (b) zonal mean precipitation (mm day^{-1}). Results shown are the differences in precipitation between CPLD2100 and CLIM2100sw (CPLD2100−CLIM2100sw). Dotted areas in (a) indicate results that are significant at the 95% level.

5.2. Aerosols

[42] Figure 16a shows year 2100 surface-layer aerosol concentrations predicted in CPLD2100. Figures 16b–16d compare impacts of future climate change by all species, GHGs, and O_3&AERs on predicted year 2100 aerosols for DJF and JJA. Future climate change driven by all species increases surface aerosol concentrations over populated areas and biomass burning regions in both DJF and JJA (Figure 16b). Climate change by O_3&AERs is as important as that by GHGs in predictions of future aerosols (Figures 16c and 16d). Over eastern China, aerosol concentrations in CPLD2100 are higher than those in CPLD2100$_{GHG}$ by 10–35 μg m^{-3} in both DJF and JJA (Figure 16d). While reduced convection owing to O_3&AERs can increase aerosol concentrations, aerosols are also influenced by reduced precipitation (wet deposition of aerosols) associated with reduced convection over populated areas (Figure 6c). Year 2100 aerosol concentrations are the highest over eastern China (Figure 16a), and O_3&AERs -induced reductions in precipitation are the largest (Figure 6c, note that the reduction in precipitation there is statistically significant), which lead to a strong positive feedback to further increase concentrations of aerosols (Figure 16d).

6. Conclusions

[43] Previous studies on the interactions between chemistry, aerosol, and climate [*Liao et al.*, 2003, 2004, 2006; *Liao and Seinfeld*, 2005; *Chen et al.*, 2007] are extended to assess the impact of full chemistry-aerosol-climate coupling on simulation of year 2100 climate and year 2100 concentrations of O_3 and aerosols. We employ the previously developed GISS GCM II' with online tropospheric ozone-NO_x-hydrocarbon chemistry and sulfate, nitrate, ammonium, black carbon, primary organic carbon, secondary organic carbon aerosols. Year 2100 concentrations of greenhouse gases as well as the anthropogenic emissions of ozone precursors and aerosols/aerosol precursors are based on IPCC scenario A2.

[44] With a fully coupled climate simulation driven by future changes in GHGs, O_3, and aerosols over 2000–2100, we predict an equilibrium increase in global mean surface air temperature of 6.1 K in DJF and of 5.8 K in JJA, and an increase in global mean precipitation by about 10% relative to that predicted for year 2000. Predicted zonal mean changes in atmospheric temperature as well as the general increases in precipitation at high latitudes and decreases in precipitation in subtropics are consistent with projections summarized by *IPCC* [2007].

[45] We have performed 5 simulations, denoted CPLD2000, CPLD2100, CHEM2100sw, CLIM2100sw, and CPLD2100$_{GHG}$, to quantify the effect of chemistry-aerosol-climate coupling on global predictions of year 2100 climate and year 2100 levels of tropospheric O_3 and aerosols. Compared with year 2100 O_3 and aerosol levels projected based on present-day climate and 2100 emissions

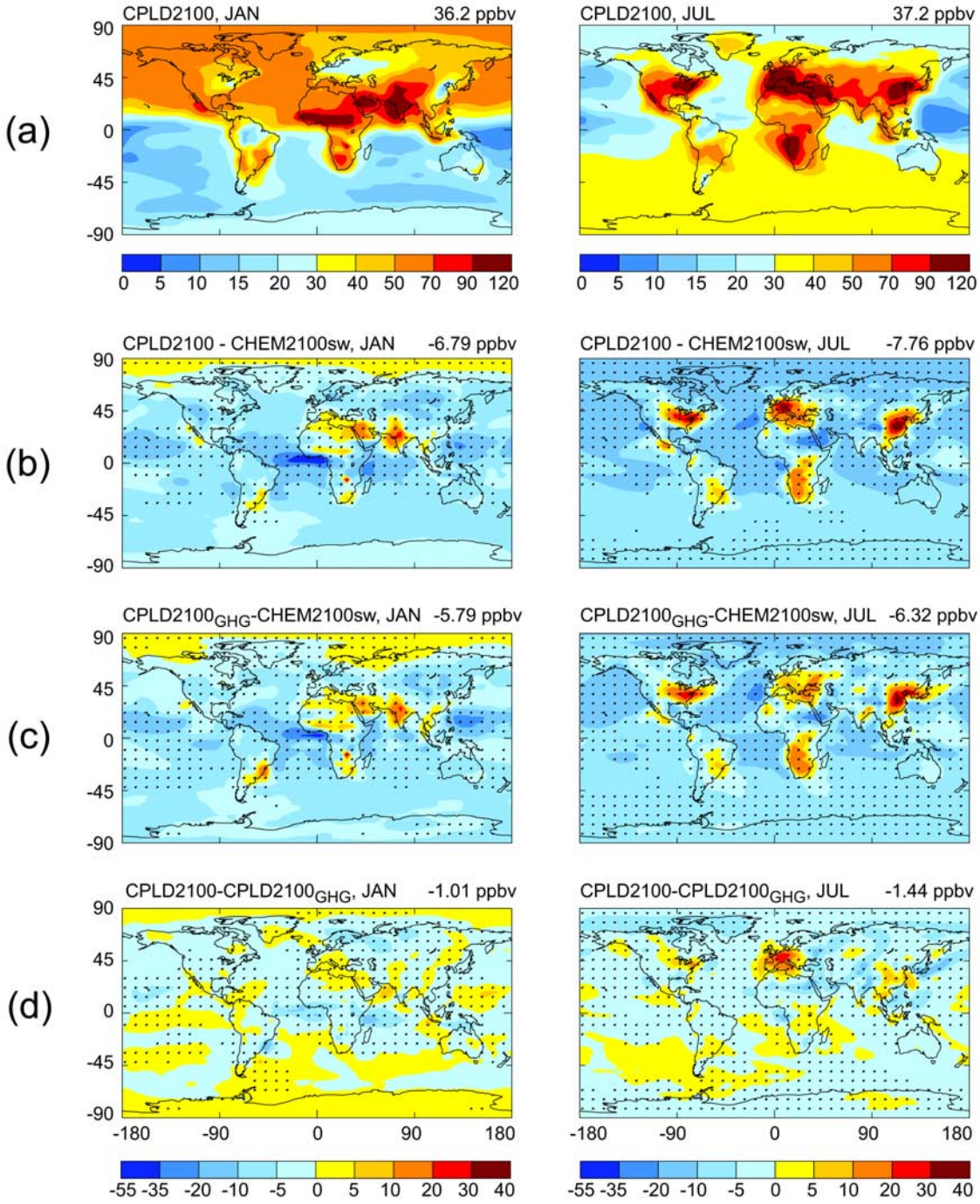

Figure 15. (a) Predicted year 2100 surface-layer O_3 mixing ratios (ppbv) for January and July in CPLD2100 based on IPCC SRES A2. (b) Effect of future climate change driven by all species on simulation of year 2100 O_3 (differences in year 2100 surface-layer O_3 mixing ratio (ppbv) between CPLD2100 and CHEM2100sw). (c) Effect of future climate change driven by GHGs alone on simulation of year 2100 O_3 ($CPLD2100_{GHG}$−CHEM2100sw). (d) Effect of future climate change driven by O_3&AERs on simulation of year 2100 O_3 (CPLD2100−$CPLD2100_{GHG}$). Left panels are for January and right panels for July. Global mean value is indicated at top right corner of each panel. Dotted areas in (b)–(d) indicate results that are significant at the 95% level.

(CHEM2100sw), the simulation with full chemistry-aerosol-climate coupling (CPLD2100) predicts: (1) a 15% lower global burden of O_3 in year 2100, as a result of the faster removal of O_3 in a warmer climate with increased water vapor content; (2) reductions in year 2100 column burden of all aerosols (including sulfate, nitrate, ammonium, BC, POA, and SOA) of 10–20 mg m^{-2} (or 40–80%) in DJF and of up to 10 mg m^{-2} (or 20–40%) in JJA in mid to high

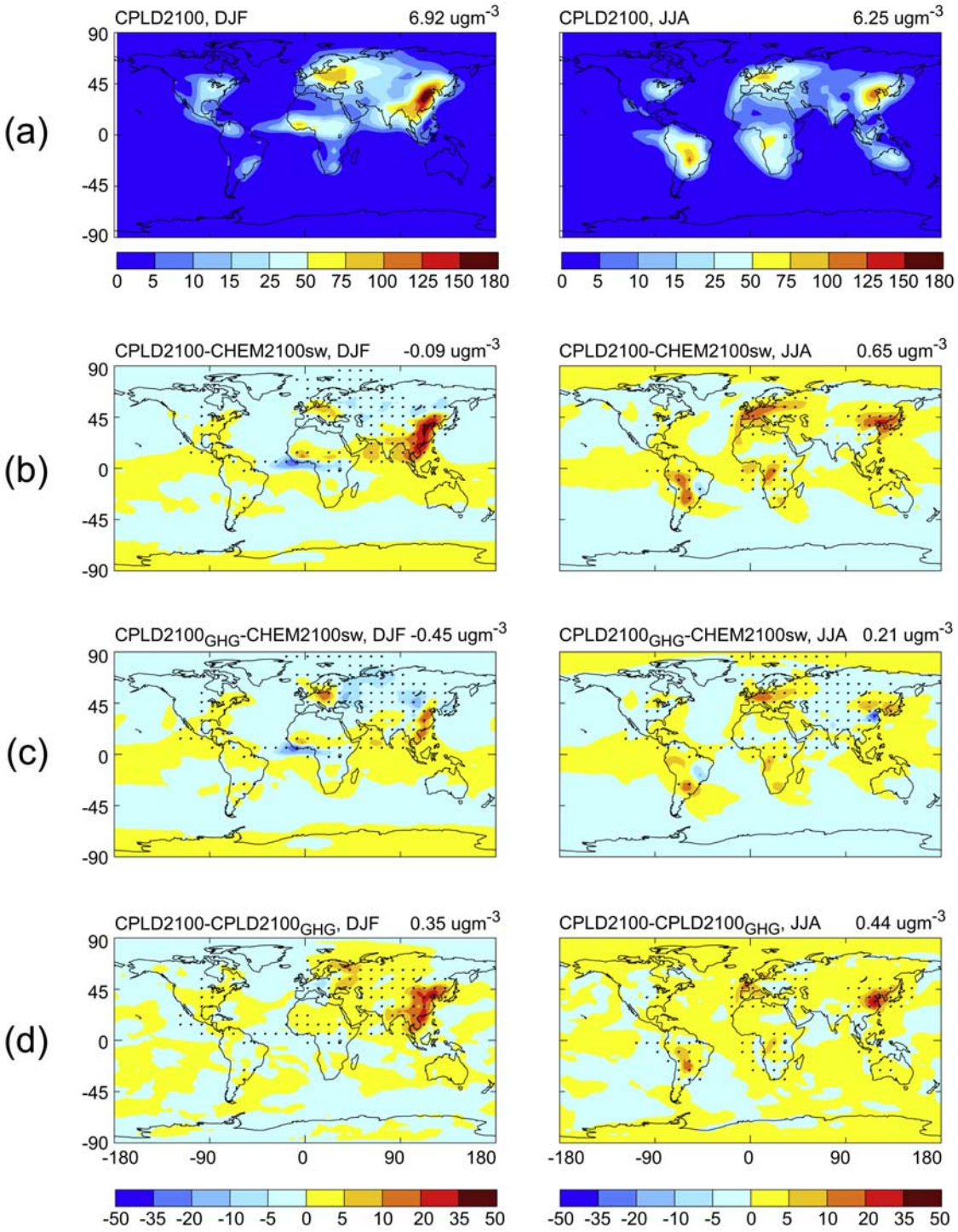

Figure 16. (a) Predicted year 2100 surface-layer all aerosol concentrations (μg m^{-3}) for DJF and JJA in CPLD2100 based on IPCC SRES A2. (a) Effect of future climate change driven by all species on simulation of year 2100 surface-layer aerosol concentrations (differences in aerosol concentrations (μg m^{-3}) between CPLD2100 and CHEM2100sw). (b) Effect of future climate change driven by GHGs alone on simulation of year 2100 surface-layer aerosol levels (CPLD2100$_{GHG}$−CHEM2100sw). (c) Effect of future climate change driven by O_3 and aerosols on simulation of year 2100 surface-layer aerosol concentrations (CPLD2100−CPLD2100$_{GHG}$). Aerosol species accounted for are sulfate, nitrate, ammonium, BC, POA, and SOA. Left panels are for DJF and right panels for JJA. Global mean value is indicated at top right corner of each panel. Dotted areas in (b)–(d) indicate results that are significant at the 95% level.

latitudes in the NH, because of the predicted increases in precipitation in year 2100; (3) lower year 2100 column burdens of all aerosols in DJF by up to 20 mg m^{-2} over the eastern United States, northeastern China, and Europe, and 30–50 mg m^{-2} increases in JJA aerosol column burdens over populated and biomass burning areas; and (4) increases in year 2100 aerosol column burdens over the tropics.

[46] Chemistry-aerosol-climate coupling has an ultimate influence on simulated year 2100 climate. Compared to the stepwise approach (CLIM2100sw) in which year 2100 climate is simulated using offline ozone and aerosol fields calculated based on present-day climate and year 2100 emissions, the fully coupled simulation (CPLD2100) predicts stronger warming in year 2100; global mean year 2100 surface air temperature simulated in CPLD2100 is higher than that obtained in CLIM2100sw by 0.44 K in DJF and by 0.41 K in JJA. Regionally, surface air temperatures simulated in CPLD2100 are higher than those obtained in CLIM2100sw by 2–4 K in DJF in NH high latitudes, by 1–2 K over Europe and eastern China in both DJF and JJA, and by 0.2–1 K over tropical oceans.

[47] We further examine the relative importance of future climate change driven by GHGs as compared to that driven by O_3 and aerosols themselves in the simulation of future O_3 and aerosols. Consideration of future GHG-driven climate change is essential for prediction of future O_3; this reproduces about 85% of future reductions in global mean O_3, and more than 80% of increases in surface O_3 over eastern China, eastern United States, southern Africa, and South America. Ozone/aerosol-driven climate change is essential for simulation of future aerosol levels, especially over populated and biomass burning areas. A strong positive feedback exists between aerosol direct radiative forcing and simulated future aerosol concentrations; high aerosol concentrations lead to reductions in convection and precipitation (or wet deposition of aerosols), further increasing aerosol concentrations in the lower troposphere.

[48] There are a number of ways in which the current study can be improved. In the present study, biogenic emissions of O_3 and SOA precursors as well as the mineral dust emissions are based on fixed vegetation and land types; these can be improved with a prognostic treatment of vegetation and land type. As shown by *Sanderson et al.* [2003] and *Lathière et al.* [2005], climate-vegetation coupling is important for predicting future biogenic hydrocarbon emissions. Second, O_3 transport from the stratosphere is fixed in all the simulations reported here; this process is climate-sensitive and should be accounted for in a more thorough treatment [*Sudo et al.*, 2003; *Collins et al.*, 2003; *Zeng and Pyle*, 2003; *Shindell et al.*, 2006a, 2006b]. Third, sea salt and mineral dust are not included here in the chemistry-aerosol-climate coupling. Fourth, because of the uncertainties inherent in using a single climate model, especially because of the coarse resolution of the GCM used in this work, comparison of results from different climate/composition models is desirable. Finally, and most importantly, aerosol indirect radiative forcing must be considered to assess complete chemistry-aerosol-climate coupling. The extent to which coupled chemical phenomena influence cloud condensation nuclei concentrations and cloud activation behavior still represents a frontier question in climate research.

[49] **Acknowledgments.** H. Liao and Y. Zhang are supported by National Natural Science Foundation of China (Grants 90711004 and 40775083) and by National Basic Research Program of China (Grant No. 2006CB403706). W.-T. Chen and J. H. Seinfeld acknowledge the support by the IDS program of NASA and the U.S. Environmental Protection Agency under Science to Achieve Results (STAR) grant RD833370. Frank Raes acknowledges support by the JRC Director General Sabbatical Programme.

References

Adams, P. J., J. H. Seinfeld, D. M. Koch, L. Mickley, and D. Jacob (2001), General circulation model assessment of direct radiative forcing by the sulfate-nitrate-ammonium-water inorganic aerosol system, *J. Geophys. Res.*, *106*, 1097–1111.

Bauer, S. E., D. Koch, N. Unger, S. M. Metzger, D. T. Shindell, and D. G. Streets (2007), Nitrate aerosols today and in 2030: A global simulation including aerosols and tropospheric ozone, *Atmos. Chem. Phys.*, *7*(19), 5043–5059.

Boer, G. J., G. Flato, and D. Ramsden (2000), A transient climate change simulation with greenhouse gas and aerosol forcing: Projected climate to the twenty-first century, *Clim. Dyn.*, *16*, 427–450.

Brasseur, G. P., J. T. Kiehl, J.-F. Müller, T. Schneider, C. Granier, X. Tie, and D. Hauglustaine (1998), Past and future changes in global tropospheric ozone: Impact on radiative forcing, *Geophys. Res. Lett.*, *25*, 3807–3810.

Brasseur, G. P., M. Schultz, C. Granier, M. Saunois, T. Diehl, M. Botzet, E. Roeckner, and S. Walters (2006), Impact of climate change on the future chemical composition of the global troposphere, *J. Clim.*, *19*(16), 3932–3951.

Chen, W.-T., H. Liao, and J. H. Seinfeld (2007), Future climate impacts of direct radiative forcing of anthropogenic aerosols, tropospheric ozone, and long-lived greenhouse gases, *J. Geophys. Res.*, *112*, D14209, doi:10.1029/2006JD008051.

Chung, S. H., and J. H. Seinfeld (2002), Global distribution and climate forcing of carbonaceous aerosols, *J. Geophys. Res.*, *107*(D19), 4407, doi:10.1029/2001JD001397.

Chung, S. H., and J. H. Seinfeld (2005), Climate response of direct radiative forcing of anthropogenic black carbon, *J. Geophys. Res.*, *110*, D11102, doi:10.1029/2004JD005441.

Chung, C. E., V. Ramanathan, and J. T. Kiehl (2002), Effects of the south Asian absorbing haze on the northeast monsoon and surface-air heat exchange, *J. Clim.*, *15*(17), 2462–2476.

Collins, W. J., R. G. Derwent, B. Garnier, C. E. Johnson, M. G. Sanderson, and D. S. Stevenson (2003), The effect of stratosphere-troposphere exchange on the future tropospheric ozone trend, *J. Geophys. Res.*, *108*(D12), 8528, doi:10.1029/2002JD002617.

Dai, A., T. M. L. Wigley, B. A. Boville, J. T. Kiehl, and L. E. Buja (2001), Climates of the twentieth and twenty-first centuries simulated by the NCAR climate system model, *J. Clim.*, *14*(4), 485–519.

Dentener, F. J., and P. J. Crutzen (1993), Reaction of N_2O_5 on tropospheric aerosols: Impact on the global distributions of NO_x, O_3, and OH, *J. Geophys. Res.*, *98*, 7149–7163.

Gauss, M., et al. (2003), Radiative forcing in the 21st century due to ozone changes in the troposphere and the lower stratosphere, *J. Geophys. Res.*, *108*(D9), 4292, doi:10.1029/2002JD002624.

Grenfell, J. L., D. T. Shindell, D. Koch, and D. Rind (2001), Chemistry-climate interactions in the Goddard Institute for Space Studies general circulation model: 2. New insights into modeling the pre-industrial atmosphere, *J. Geophys. Res.*, *106*, 33,435–33,451.

Griffin, R. J., D. R. Cocker, J. H. Seinfeld, and D. Dabdub (1999a), Estimate of global atmospheric organic aerosol from oxidation of biogenic hydrocarbons, *Geophy. Res. Lett.*, *26*, 2721–2724.

Griffin, R. J., D. R. Cocker, R. C. Flagan, and J. H. Seinfeld (1999b), Organic aerosol formation from the oxidation of biogenic hydrocarbons, *J. Geophys. Res.*, *104*, 3555–3567.

Guenther, A., T. Karl, P. Harley, C. Wiedinmyer, P. I. Palmer, and C. Geron (2006), Estimates of global terrestrial isoprene emissions using MEGAN (Model of Emissions of Gases and Aerosols from Nature), *Atmos. Chem. Phys.*, *6*(11), 3181–4055.

Hansen, J., A. Lacis, G. Russell, P. Stone, I. Fung, R. Ruedy, and J. Lerner (1984), Climate sensitivity: Analysis of feedback mechanisms, in *Climate Processes and Climate Sensitivity*, *Geophys. Monogr. Ser.*, vol. 29, edited by J. E. Hansen and T. Takahashi, pp. 130–163, AGU, Washington, D. C.

Hansen, J., M. Sato, and R. Ruedy (1997), Radiative forcing and climate response, *J. Geophys. Res.*, *102*, 6831–6864.
Hansen, J., et al. (2005), Efficacy of climate forcings, *J. Geophys. Res.*, *110*, D18104, doi:10.1029/2005JD005776.
Hogrefe, C., B. Lynn, K. Civerolo, J.-Y. Ku, J. Rosenthal, C. Rosenzweig, R. Goldberg, S. Gaffin, K. Knowlton, and P. L. Kinney (2004), Simulating changes in regional air pollution over the eastern United States due to changes in global and regional climate and emissions, *J. Geophys. Res.*, *109*, D22301, doi:10.1029/2004JD004690.
Horowitz, L. W. (2006), Past, present, and future concentrations of tropospheric ozone and aerosols: Methodology, ozone evaluation, and sensitivity to aerosol wet removal, *J. Geophys. Res.*, *111*, D22211, doi:10.1029/2005JD006937.
IPCC (2007), *Climate Change 2007: The Physical Science Basis*, Cambridge Univ. Press, Cambridge, U. K.
Iversen, T., and Ø. Seland (2002), A scheme for process-tagged SO_4 and BC aerosols in NCAR CCM3: Validation and sensitivity to cloud processes, *J. Geophys. Res.*, *107*(D24), 4751, doi:10.1029/2001JD000885.
Jacob, D. J. (2000), Heterogeneous chemistry and tropospheric ozone, *Atmos. Environ.*, *34*, 2131–2159.
Jacobson, M. Z. (1998), Studying the effects of aerosols on vertical photolysis rate coefficient and temperature profiles over an urban airshed, *J. Geophys. Res.*, *103*, 10,593–10,604.
Jacobson, M. Z. (2004), Climate response of fossil fuel and biofuel soot, accounting for soot's feedback to snow and sea ice albedo and emissivity, *J. Geophys. Res.*, *109*, D21201, doi:10.1029/2004JD004945.
Johnson, C. E., W. J. Collins, D. S. Stevenson, and R. G. Derwent (1999), Relative roles of climate and emissions changes on future tropospheric oxidant concentrations, *J. Geophys. Res.*, *104*, 18,631–18,645.
Johnson, C. E., D. S. Stevenson, W. J. Collins, and R. G. Derwent (2001), Role of climate feedback on methane and ozone studied with a coupled Ocean-Atmosphere-Chemistry model, *Geophys. Res. Lett.*, *28*, 1723–1726.
Koch, D. M. (2001), Transport and direct radiative forcing of carbonaceous and sulfate aerosols in the GISS GCM, *J. Geophys. Res.*, *106*, 20,311–20,332.
Lathière, J., D. A. Hauglustaine, N. deNoblet-Ducoudré, G. Krinner, and G. A. Folberth (2005), Past and future changes in biogenic volatile organic compound emissions simulated with a global dynamic vegetation model, *Geophys. Res. Lett.*, *32*, L20818, doi:10.1029/2005GL024164.
Levy, H., II, M. D. Schwarzkopf, L. Horowitz, V. Ramaswamy, and K. L. Findell (2008), Strong sensitivity of late 21st century climate to projected changes in short-lived air pollutants, *J. Geophys. Res.*, *113*, D06102, doi:10.1029/2007JD009176.
Liao, H., and J. H. Seinfeld (2005), Global impacts of gas-phase chemistry-aerosol interactions on direct radiative forcing by anthropogenic aerosols and ozone, *J. Geophys. Res.*, *110*, D18208, doi:10.1029/2005JD005907.
Liao, H., Y. L. Yung, and J. H. Seinfeld (1999), Effects of aerosols on tropospheric photolysis rates in clear and cloudy atmospheres, *J. Geophys. Res.*, *104*, 23,697–23,707.
Liao, H., P. J. Adams, S. H. Chung, J. H. Seinfeld, L. J. Mickley, and D. J. Jacob (2003), Interactions between tropospheric chemistry and aerosols in a unified general circulation model, *J. Geophys. Res.*, *108*(D1), 4001, doi:10.1029/2001JD001260.
Liao, H., J. H. Seinfeld, P. J. Adams, and L. J. Mickley (2004), Global radiative forcing of coupled tropospheric ozone and aerosols in a unified general circulation model, *J. Geophys. Res.*, *109*, D16207, doi:10.1029/2003JD004456.
Liao, H., W.-T. Chen, and J. H. Seinfeld (2006), Role of climate change in global predictions of future tropospheric ozone, and aerosols, *J. Geophys. Res.*, *111*, D12304, doi:10.1029/2005JD006852.
Meehl, G. A., et al. (2007), Global Climate Projections, in *Climate Change 2007: The Physical Science Basis. Contribution of Working Group I to the Fourth Assessment Report of the Intergovernmental Panel on Climate Change*, edited by S. Solomon et al., chap. 10, pp. 747–846, Cambridge Univ. Press, Cambridge, U. K.
Menon, S. (2004), Current uncertainties in assessing aerosol effects on climate, *Annu. Rev. Environ. Res.*, *29*(1), 1–30.
Menon, S., J. Hansen, L. Nazarenko, and Y. F. Luo (2002), Climate effects of black carbon aerosols in China and India, *Science*, *297*(5590), 2250–2253.
Mickley, L. J., D. J. Jacob, B. D. Field, and D. Rind (2004), Climate response to the increase in tropospheric ozone since preindustrial times: A comparison between ozone and equivalent CO_2 forcings, *J. Geophys. Res.*, *109*, D05106, doi:10.1029/2003JD003653.
Mitas, C. M., and A. Clement (2006), Recent behavior of the Hadley cell and tropical thermodynamics in climate models and reanalyses, *Geophys. Res. Lett.*, *33*, L01810, doi:10.1029/2005GL024406.
Mitchell, J. F. B. (1989), The "greenhouse" effect and climate change, *Rev. Geophys.*, *27*, 115–139.
Murazaki, K., and P. Hess (2006), How does climate change contribute to surface ozone change over the United States?, *J. Geophys. Res.*, *111*, D05301, doi:10.1029/2005JD005873.
Nakicenovic, N., et al. (2000), *Emissions Scenarios. A Special Report of Working Group III of the Intergovernmental Panel on Climate Change*, 599 pp., Cambridge Univ. Press, New York.
Nenes, A., C. Pilinis, and S. N. Pandis (1998), Isorropia: A new thermodynamic equilibrium model for multiphase multicomponent inorganic aerosols, *Aquat. Geochem.*, *4*, 123–152.
Price, C., and D. Rind (1992), Possible implications of global climate change on global lightning distributions and frequencies, *J. Geophys. Res.*, *99*, 10,823–10,831.
Pye, H. O. T., H. Liao, S. Wu, L. J. Mickley, D. J. Jacob, D. K. Henze, and J. H. Seinfeld (2009), Effect of changes in climate and emissions on future sulfate-nitrate-ammonium aerosol levels in the United State, *J. Geophys. Res.*, *114*, D01205, doi:10.1029/2008JD010701.
Racherla, P. N., and P. J. Adams (2008), The response of surface ozone to climate change over the Eastern United States, *Atmos. Chem. Phys.*, *8*(4), 871–885.
Ramanathan, V., C. Chung, D. Kim, T. Bettge, L. Buja, J. T. Kiehl, W. M. Washington, Q. Fu, D. R. Sikka, and M. Wild (2005), Atmospheric brown clouds: Impacts on South Asian climate and hydrological cycle, *Proc. Natl. Acad. Sci.*, *102*(15), 5326–5333.
Ramaswamy, V., and M. M. Bowen (1994), Effect of changes in radiatively active species upon the lower stratospheric temperatures, *J. Geophys. Res.*, *99*(D9), 18,909–18,921.
Rind, D., and J. Lerner (1996), The use of on-line tracers as a diagnostic tool in general circulation model development: 1. Horizontal and vertical transport in the troposphere, *J. Geophys. Res.*, *101*, 12,667–12,683.
Rind, D., J. Lerner, K. Shah, and R. Suozzo (1999), Use of on-line tracers as a diagnostic tool in general circulation model development: 2. Transport between the troposphere and stratosphere, *J. Geophys. Res.*, *104*, 9151–9167.
Rind, D., J. Lerner, and C. McLinden (2001), Changes of tracer distribution in the doubled CO2 climate, *J. Geophys. Res.*, *106*, 28,061–28,080.
Roeckner, E., P. Stier, J. Feichter, S. Kloster, M. Esch, and I. Fischer-Bruns (2006), Impact of carbonaceous aerosol emissions on regional climate change, *Clim. Dynam.*, *27*, 553–571.
Russell, G. L., J. R. Miller, and L.-C. Tsang (1984), Seasonal ocean heat transports computed from an atmospheric model, *Dynam. Atmos. Oceans*, *9*, 253–271.
Sanderson, M. G., C. D. Jones, W. J. Collins, C. E. Johnson, and R. G. Derwent (2003), Effect of climate change on isoprene emissions and surface ozone levels, *Geophys. Res. Lett.*, *30*(18), 1936, doi:10.1029/2003GL017642.
Shindell, D. T., J. L. Grenfell, D. Rind, V. Grewe, and C. Price (2001), Chemistry-climate interactions in the Goddard Institute for Space Studies general circulation model: 1. Tropospheric chemistry model description and evaluation, *J. Geophys. Res.*, *106*, 8047–8075.
Shindell, D., G. Faluvegi, A. Lacis, J. Hansen, and R. Ruedy (2006a), Role of tropospheric ozone increases in 20th-century climate change, *J. Geophys. Res.*, *111*, D08302, doi:10.1029/2005JD006348.
Shindell, D. T., G. Faluvegi, N. Unger, E. Aguilar, G. A. Schmidt, D. Koch, S. E. Bauer, and R. L. Miller (2006b), Simulations of preindustrial, present-day, and 2100 conditions in the NASA GISS composition and climate model G-PUCCINI, *Atmos. Chem. Phys.*, *6*, 4427–4459.
Shindell, D. T., H. Levy II, M. D. Schwarzkopf, L. W. Horowitz, J.-F. Lamarque, and G. Faluvegi (2008), Multimodel projections of climate change from short-lived due to human activities, *J. Geophys. Res.*, *113*, D11109, doi:10.1029/2007JD009152.
Steiner, A. L., S. Tonse, R. C. Cohen, A. H. Goldstein, and R. A. Harley (2006), Influence of future climate and emissions on regional air quality in California, *J. Geophys. Res.*, *111*, D18303, doi:10.1029/2005JD006935.
Stevenson, D. S., et al. (2006), Multimodel ensemble simulations of present-day and near-future tropospheric ozone, *J. Geophys. Res.*, *111*, D08301, doi:10.1029/2005JD006338.
Stier, P., J. Feichter, E. Roeckner, S. Kloster, and M. Esch (2006), The evolution of the global aerosol system in a transient climate simulation from 1860 to 2100, *Atmos. Chem. Phys.*, *6*, 3059–3076.
Stuber, N., M. Ponater, and R. Sausen (2001), Is the climate sensitivity to ozone perturbations enhanced by stratospheric water vapor feedback?, *Geophys. Res. Lett.*, *28*(15), 2887–2890.
Sudo, K., M. Takahashi, and H. Akimoto (2003), Future changes in stratosphere-troposphere exchange and their impacts on future tropospheric ozone simulations, *Geophys. Res. Lett.*, *30*(24), 2256, doi:10.1029/2003GL018526.
Takemura, T., T. Nozawa, and S. Emori (2005), Simulation of climate response to aerosol direct and indirect effects with aerosol transport-

radiation model, *J. Geophys. Res.*, *11*, D02202, doi:10.1029/2004JD005029.

Unger, N., D. T. Shindell, D. M. Koch, M. Amann, J. Cofala, and D. G. Streets (2006), Influences of man-made emissions and climate changes on tropospheric ozone, methane, and sulfate at 2030 from a broad range of possible futures, *J. Geophys. Res.*, *111*, D12313, doi:10.1029/2005JD006518.

Wang, C. (2004), A modeling study on the climate impacts of black carbon aerosols, *J. Geophys. Res.*, *109*, D03106, doi:10.1029/2003JD004084.

Wang, C. (2007), Impact of direct radiative forcing of black carbon aerosols on tropical convective precipitation, *Geophys. Res. Lett.*, *34*, L05709, doi:10.1029/2006GL028416.

Wang, Y., D. J. Jacob, and J. A. Logan (1998), Global simulation of tropospheric O_3-NO_x-hydrocarbon chemistry: 1. Model formulation, *J. Geophys. Res.*, *103*(D9), 10,713–10,725.

Wiedinmyer, C., X. Tie, A. Guenther, R. Neilson, and C. Granier (2006), Future changes in biogenic isoprene emissions: How might they affect regional and global atmospheric chemistry?, *Earth Interact.*, *10*(3), EI174, doi:10.1175/EI174.1.

Wu, S., L. J. Mickley, E. M. Leibensperger, D. J. Jacob, D. Rind, and D. G. Streets (2008), Effects of 2000–2050 global change on ozone air quality in the United States, *J. Geophys. Res.*, *113*, D06302, doi:10.1029/2007JD008917.

Zeng, G., and J. A. Pyle (2003), Changes in tropospheric ozone between 2000 and 2100 modeled in a chemistry-climate model, *Geophys. Res. Lett.*, *30*(7), 1392, doi:10.1029/2002GL016708.

W.-T. Chen and J. H. Seinfeld, Department of Environmental Science and Engineering, California Institute of Technology, Mail Code 210-41, 1200 E. California Boulevard, Pasadena, CA 91125, USA.

H. Liao and Y. Zhang, LAPC, Institute of Atmospheric Physics, Chinese Academy of Sciences, Beijing 100029, China. (hongliao@mail.iap.ac.cn)

F. Raes, European Commission, Joint Research Center, 21020 Ispra (VA), Italy.